Steering Control of an Autonomous Unicycle

Máté B. Vizi, Gábor Orosz, *Senior Member, IEEE*, Dénes Takács, and Gábor Stépán

***Abstract*—The steering control of an autonomous unicycle is considered. The underlying dynamical model of a single rolling wheel is discussed regarding the steady-state motions and their stability. The unicycle model is introduced as the simplest possible extension of the rolling wheel, where the location of the center of gravity is controlled. With the help of the Appellian approach, a state-space representation of the controlled nonholonomic system is built in a way that the most compact nonlinear equations of motion are constructed. Based on controllability analysis, feedback controllers are designed that successfully carry out lane changing and turning maneuvers. The behavior of the closed-loop system is demonstrated by numerical simulations.**

***Index Terms*—Feedback control, maneuvering, nonholonomic dynamics, stability, unicycle.**

I. Introduction

MICROMOBILITY solutions are spreading rapidly in urban environments [1]. Among these, human-ridden electric unicycles (EUCs) become more and more popular transportation devices [see Fig. 1(a)]. These micromobility vehicles can match the speed of automobiles in urban traffic, while their compact size makes them appealing for commuting in congested environments. Due to the 3-D spatial rolling of the wheel and the stabilization of an unstable equilibrium, the unique dynamics of the unicycle combine agility and maneuverability. To exploit these properties, one may consider making EUCs autonomous [see Fig. 1(b)], which opens up a challenging avenue for modeling, dynamics, and control.

During the last few decades, several autonomous unicycle designs have appeared in the literature that differ in various aspects, such as the number and/or types of actuators that can be used for control. The first publication related to autonomous unicycles known to the authors is [2] in which the longitudinal/pitch motion is controlled by balancing an inverted pendulum, and the lateral/tilt motion is controlled by moving a mass perpendicular to the wheel. Two other approaches are presented in [3]. In the first case, the longitudinal/pitch motion is also controlled by balancing an inverted pendulum, while the turning/yaw motion of the unicycle is controlled by an overhead flywheel. In the second case, the tilt is controlled by adding a second pendulum swinging in the lateral plane. The overhead flywheel approach was further explored in [4] and [5]; the lateral pendulum approach can be found in [6]. The tilt motion of the unicycle can also be controlled by a lateral flywheel (see, for example, [7], [8], [9]), while the combination of overhead and lateral flywheels can be found in [10] and [11]. Furthermore, the application of gyroscopes for lateral stabilization and steering is presented in [12], [13], [14], and [15]. Humanoid-type autonomous unicycles are introduced and analyzed in [16] and [17] (see Fig. 1(a) for illustration).

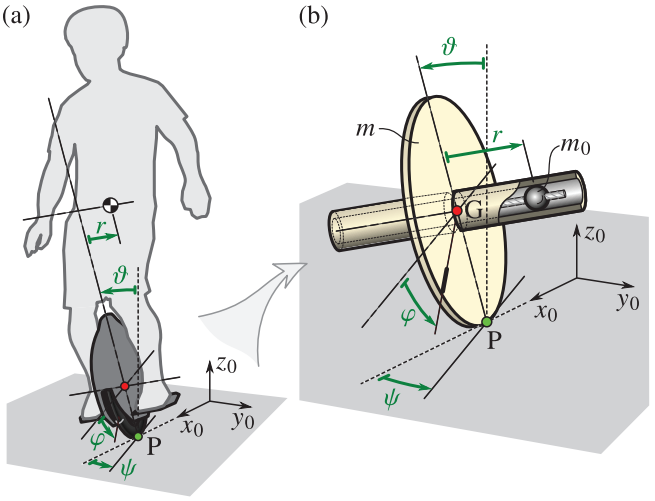

Fig. 1. (a) Human riding a unicycle and (b) simple autonomous EUC.

Most of the above approaches provide satisfactory dynamic behavior, but their complexity prohibits closed-form analysis of the controlled system. Our goal here is to develop a simple autonomous unicycle model that is capable of carrying out a variety of maneuvers, while it can still be investigated analytically. Thus, we consider the simple mechanical model shown in Fig. 1(b), which consists of a rolling wheel and added mass that can be moved along the axle to balance the lateral motion. We derive the equations of motion for this simple system, analyze the stability properties, and design controllers for maneuvering the autonomous unicycle.

Received 29 June 2024; revised 25 February 2025; accepted 4 July 2025. Date of publication 3 October 2025; date of current version 23 October 2025. This work was supported in part by the Hungarian National Science Foundation under Grant NKFI K 132477 and Grant NKFI KKP 133846, in part by the HUN-REN Hungarian Research Network, and in part by the Ministry of Culture and Innovation of Hungary through the National Research, Development and Innovation Fund as part of the TKP2021-NVA Funding Scheme under Project TKP-6-6/PALY-2021. The work of Gábor Orosz was supported in part by the Hungarian Academy of Sciences within the Distinguished Guest Fellowship Programme 2022 and in part by the Fulbright Foundation 2023–2024. The work of Dénes Takács was supported by the Hungarian Academy of Sciences through a János Bolyai Research Scholarship. Recommended by Associate Editor J. B. Hoagg. *(Corresponding author: Máté B. Vizi.)*

Máté B. Vizi is with the Department of Mechanical Engineering, University of Michigan, Ann Arbor, MI 48109 USA, and also with the HUN-REN-BME Dynamics of Machines Research Group, 1111 Budapest, Hungary (e-mail: vizi@mm.bme.hu).

Gábor Orosz is with the Department of Mechanical Engineering and the Department of Civil and Environmental Engineering, University of Michigan, Ann Arbor, MI 48109 USA (e-mail: orosz@umich.edu).

Dénes Takács and Gábor Stépán are with the Department of Applied Mechanics, Budapest University of Technology and Economics, 1111 Budapest, Hungary, and also with the HUN-REN–BME Dynamics of Machines Research Group, 1111 Budapest, Hungary (e-mail: takacs@mm.bme.hu; stepan@mm.bme.hu).

Digital Object Identifier 10.1109/TCST.2025.3587096

The rolling of the wheel can be described using kinematic constraints [18], [19], [20], [21]. Thus, the unicycle is considered a nonholonomic mechanical system. Such systems are often described by the generalized Lagrangian equations of the second kind (or Routh–Voss equations) [22], [23]. This method yields a differential–algebraic system of equations. However, eliminating the algebraic variables to obtain a system of ordinary differential equations that is appropriate for control design is a challenging task. Alternatively, for conservative nonholonomic systems, a Routhian-like model reduction technique, the so-called Lagrange–d'Alembert–Poincaré equations can be used to identify conserved quantities and also to explore symmetries [24].

The Appellian approach [21], [25], [26], which is used in this study, results in a system of first-order ordinary differential equations as a compact and simple representation of the underlying nonholonomic system. Moreover, an innovative definition of the pseudovelocities can significantly reduce the algebraic complexity of the resulting equations of motion while describing the same dynamical system, which simplifies the subsequent analysis. This enables one to deploy a plethora of control techniques. The cost of the Appellian formalism is that accelerations must be calculated; however, the mentioned benefits justify this cost in the examples considered here.

Further details about nonholonomic systems may be found in [27], [28], [29], [30], [31], [32], [33], and [34].

In this study, we first omit the mass moving along the axle in Fig. 1(b) and explore the dynamics of the uncontrolled rolling wheel. We categorize different steady-state motions (e.g., straight rolling and turning) of interest. A strong sufficient condition of stable rolling was given by Bloch in [34], while here the local necessary and sufficient condition is derived. This simplified case also enables us to explain the self-stabilizing effects in the tilt direction above a critical speed. By adding the moving mass and an internal force between the wheel and the mass, we create a control system and study how the steady states are affected. This enables us to design feedback controllers that stabilize the steady states at any speed and enables the unicycle to perform maneuvers such as lane changes and sharp turns. Our control design exploits the inherent instabilities of the system to demonstrate a high level of maneuverability.

The article is structured as follows. In Section II, the modeling framework and steady-state analysis of the rolling wheel example are presented. Section III introduces a novel autonomous unicycle model and analyzes the steady states of the open-loop system. Section IV proposes controller designs that successfully perform lane changing and turning maneuvers. The performance of these controllers is demonstrated by numerical simulations. We conclude our results in Section V and provide future research directions.

II. Dynamics of the Rolling Wheel

We introduce the modeling framework and notation on the rolling wheel example, which represents the uncontrolled behavior of the unicycle. We reveal the dynamical characteristics, including the self-stabilization phenomenon, which can be exploited for control design.

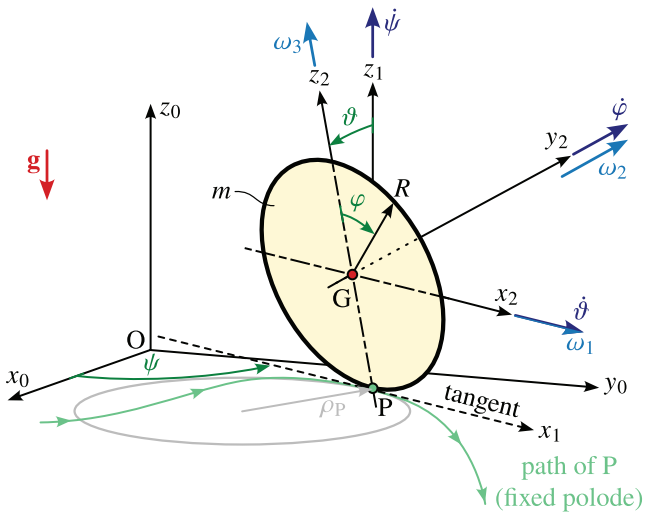

Fig. 2. Mechanical model of the rolling wheel.

A. Governing Equations

A wheel has $N = 6$ degrees of freedom (DoFs) in the 3-D space. That is, the spatial position and orientation are described by six variables: the position of the center of gravity $\mathbf{r}_G = [x_G \;\; y_G \;\; z_G]^\top$ and the yaw (ψ), tilt (ϑ), and pitch (φ) angles (see Fig. 2). Note that tilt is often called roll in the vehicle dynamics literature, but here we do not use this convention to avoid confusion with the fact that a disk rolls on the horizontal plane.

To describe the motion of the wheel, three coordinate frames are introduced (see Fig. 2). The axes x_0 and y_0 of the ground-fixed frame F_0 span the horizontal plane, and its z_0-axis gives the vertical direction. The frame F_1 is moving with the wheel such that its origin is the wheel–ground contact point P. This frame is rotated with respect to F_0 around the z_0-axis with the yaw angle ψ so that the x_1-axis is tangential to the path of P (the fixed polode). The frame F_2 is rotated with respect to F_1 around the x_1-axis with the tilt angle ϑ, so the x_1- and z_1-axes span the plane of the wheel and the y_2-axis is aligned with the wheel axle. The origin of frame F_2 is placed at the wheel center point G.

Assume that the wheel rolls without slipping; the kinematic condition of rolling is that the instantaneous center of rotation coincides with the contact point P

$$\mathbf{v}_P = \mathbf{0}\,. \tag{1}$$

This yields the kinematic constraints

$$\begin{aligned} \dot{x}_G &= \dot{\psi} R\cos\psi\sin\vartheta + \dot{\vartheta} R\sin\psi\cos\vartheta + \dot{\varphi} R\cos\psi\,,\\ \dot{y}_G &= \dot{\psi} R\sin\psi\sin\vartheta - \dot{\vartheta} R\cos\psi\cos\vartheta + \dot{\varphi} R\sin\psi\,, \end{aligned} \tag{2}$$

and the geometric constraint

$$\dot{z}_G = -R\dot{\vartheta}\sin\vartheta \quad\Rightarrow\quad z_G = R\cos\vartheta\,, \tag{3}$$

where the vertical position z_G depends on the tilt angle ϑ (see Fig. 2). Therefore, the rolling wheel is a nonholonomic mechanical system with $n_g = 1$ geometric constraint (3) and $n_k = 2$ kinematic constraints (2). Note that the geometric and kinematic constraints are also referred to as holonomic

and nonholonomic constraints, respectively. The equations of motion are derived in Appendix A using the Appellian approach [21], [25], [26] to provide the most compact algebraic form.

According to the number of geometric and kinematic constraints, $n_q = 6 - n_g = 5$ generalized coordinates have to be chosen to describe the system unambiguously; let these be

$$(x_G,\, y_G,\, \psi,\, \vartheta,\, \varphi)\ . \tag{4}$$

Moreover, $n_\sigma = n_q - n_k = 3$ pseudovelocities have to be chosen; let these be defined by the components of the angular velocity $\boldsymbol{\omega}$ resolved in frame F_2 (see (73) in Appendix A)

$$\omega_1 := \dot{\vartheta}, \quad \omega_2 := \dot{\psi}\sin\vartheta + \dot{\varphi}, \quad \omega_3 := \dot{\psi}\cos\vartheta. \tag{5}$$

Then, the Appellian approach yields the equations of motion

$$\begin{cases} \dot{\omega}_1 = \dfrac{6}{5}\omega_2\omega_3 - \dfrac{1}{5}\omega_3^2\tan\vartheta + \dfrac{4g}{5R}\sin\vartheta\,, \\ \dot{\omega}_2 = -\dfrac{2}{3}\omega_1\omega_3\,, \\ \dot{\omega}_3 = -2\omega_1\omega_2 + \omega_1\omega_3\tan\vartheta\,, \\ \dot{\vartheta} = \omega_1\,, \end{cases}$$
$$\begin{cases} \dot{\psi} = \omega_3\dfrac{1}{\cos\vartheta}\,, \\ \dot{\varphi} = \omega_2 - \omega_3\tan\vartheta\,, \\ \dot{x}_G = \omega_1 R\sin\psi\cos\vartheta + \omega_2 R\cos\psi\,, \\ \dot{y}_G = -\omega_1 R\cos\psi\cos\vartheta + \omega_2 R\sin\psi\,, \end{cases} \tag{6}$$

that is, the rolling wheel is an $n = 6 - n_g - n_k/2 = 4$ DoF nonholonomic mechanical system. The equations in (6) are ordered such that the system can be separated into essential dynamics (the first four equations) and hidden dynamics (the second four equations) where the essential dynamics is independent of the hidden dynamics [22]. The equations are in the form $\dot{\mathbf{x}} = f(\mathbf{x})$ where the state is defined as

$$\mathbf{x} = \left[\begin{array}{cccc|cccc} \omega_1 & \omega_2 & \omega_3 & \vartheta & \psi & \varphi & x_G & y_G \end{array}\right]^\top, \tag{7}$$

where the dashed line separates the essential states from the cyclic coordinates describing hidden motion.

B. Steady-State Motions

The rolling wheel exhibits a steady-state motion when the essential dynamics [first four equations in (6)] possess an equilibrium. That is, the pseudovelocities and the tilt angle are constants

$$\omega_1(t) \equiv \omega_{1*}\,,\ \omega_2(t) \equiv \omega_{2*}\,,\ \omega_3(t) \equiv \omega_{3*}\,,\ \vartheta(t) \equiv \vartheta_*\,. \tag{8}$$

Then, according to the fourth equation in (6), the tilt rate must be zero, that is, $\omega_{1*} = 0$. Substituting this into (6), the first equation yields

$$\frac{6}{5}\omega_{2*}\omega_{3*} - \frac{1}{5}\omega_{3*}^2\tan\vartheta_* + \frac{4g}{5R}\sin\vartheta_* = 0\,, \tag{9}$$

while the hidden motion can be expressed as

$$\dot{\psi}(t) \equiv \dot{\psi}_* = \omega_{3*}\frac{1}{\cos\vartheta_*}\,, \qquad \dot{x}_G(t) = \omega_{2*}R\cos\psi(t)\,,$$
$$\dot{\varphi}(t) \equiv \dot{\varphi}_* = \omega_{2*} - \omega_{3*}\tan\vartheta_*\,, \quad \dot{y}_G(t) = \omega_{2*}R\sin\psi(t)\,. \tag{10}$$

That is, the yaw rate $\dot{\psi}$ and the pitch rate $\dot{\varphi}$ are constants, while the horizontal velocity components $\dot{x}_G$ and $\dot{y}_G$ of the center of gravity vary with time through the yaw angle ψ.

Integrating (10), the generalized coordinates become

$$\psi_*(t) = \dot{\psi}_* t + \psi_0\,,$$
$$\varphi_*(t) = \dot{\varphi}_* t + \varphi_0\,,$$
$$x_{G*}(t) = \begin{cases} \left(\dfrac{\dot{\varphi}_*}{\dot{\psi}_*} + \sin\vartheta_*\right) R\sin\left(\dot{\psi}_* t + \psi_0\right) + x_0 & \text{if } \dot{\psi}_* \neq 0\,, \\ \dot{\varphi}_* t R\cos\psi_0 + x_0 & \text{if } \dot{\psi}_* = 0\,, \end{cases}$$
$$y_{G*}(t) = \begin{cases} -\left(\dfrac{\dot{\varphi}_*}{\dot{\psi}_*} + \sin\vartheta_*\right) R\cos\left(\dot{\psi}_* t + \psi_0\right) + y_0 & \text{if } \dot{\psi}_* \neq 0\,, \\ \dot{\varphi}_* t R\sin\psi_0 + y_0 & \text{if } \dot{\psi}_* = 0\,, \end{cases} \tag{11}$$

where ψ_0 and φ_0 denote the initial yaw and pitch angles, while x_0 and y_0 originate in the initial position of point G. The center of gravity G follows a circular path of radius $\rho_G = |\dot{\varphi}_*/\dot{\psi}_* + \sin\vartheta_*|R$ if the yaw rate is not zero ($\dot{\psi}_* \neq 0$). Correspondingly, the contact point P draws a circle of radius $\rho_P = |\dot{\varphi}_*/\dot{\psi}_*|R$ on the ground plane (see Fig. 2). We refer to this motion as turning-rolling in the rest of the article. For zero yaw rate ($\dot{\psi}_* = 0$), the center of gravity moves along a straight path. We refer to this as straight rolling in the rest of the article.

Keep in mind that the steady-state tilt angle, yaw rate, and pitch rate are not independent of each other. To establish a relationship between these quantities, one must replace the steady-state pseudovelocities (ω_{1*}, ω_{2*}, ω_{3*}) in (9) with the generalized velocities ($\dot{\psi}_*$, $\dot{\varphi}_*$) according to (5). This yields

$$\dot{\psi}_*^2\sin\vartheta_*\cos\vartheta_* + \frac{6}{5}\dot{\psi}_*\dot{\varphi}_*\cos\vartheta_* + \frac{4g}{5R}\sin\vartheta_* = 0\,, \tag{12}$$

which is visualized in Fig. 3(a). Since (12) is linear in the pitch rate $\dot{\varphi}_*$, one may express $\dot{\varphi}_*$ as a function of the tilt angle ϑ_* and the yaw rate $\dot{\psi}_*$ for turning-rolling ($\dot{\psi}_* \neq 0$).

For straight rolling ($\dot{\psi}_* = 0$), (12) reduces to

$$\sin\vartheta_* = 0\,, \tag{13}$$

yielding $\vartheta_* = 0$, that is, the wheel must be nontilted. Observe that (13) is independent of the pitch rate $\dot{\varphi}_*$, so the straight rolling is feasible for arbitrary pitch rates. Another special case is when the pitch rate is zero ($\dot{\varphi}_* = 0$). Then, (12) results in

$$\dot{\psi}_*^2\sin\vartheta_*\cos\vartheta_* + \frac{4g}{5R}\sin\vartheta_* = 0\,, \tag{14}$$

which can only hold when the tilt angle is zero, that is, $\vartheta_* = 0$. We refer to this solution as spinning on the spot in the rest of the article. Finally, the very special case $\dot{\psi}_* = \dot{\varphi}_* = 0$ corresponds to the static equilibrium of the standing disk, which is, indeed, unstable.

The stability of the steady states (turning-rolling, straight rolling, and spinning) is analyzed consecutively below.

C. Stability of the Steady-State Motions

The steady-state motions of the rolling wheel are defined with respect to the essential motion independent

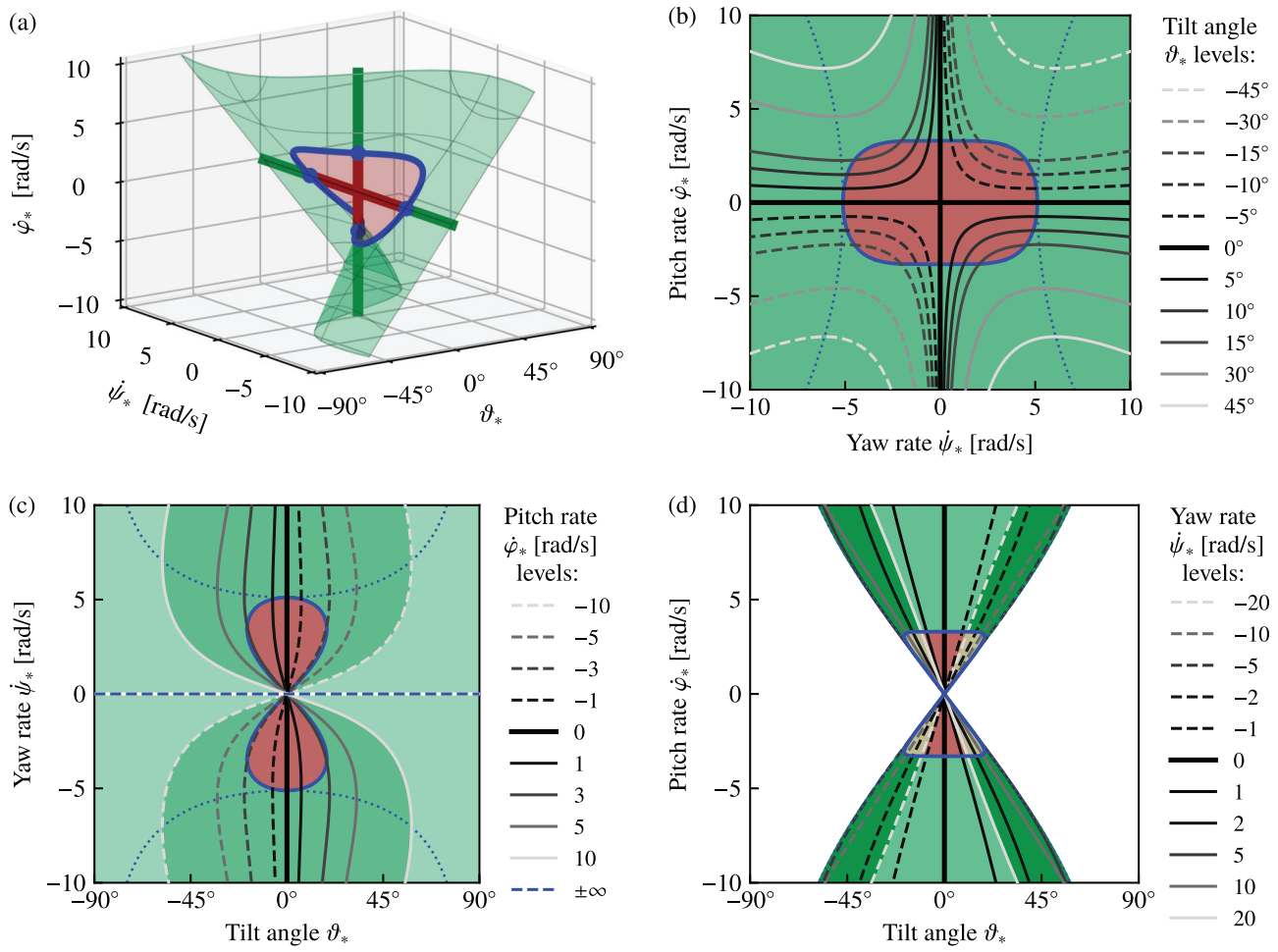

Fig. 3. Level sets and stability of steady-state motion (12) of the rolling wheel: stable and unstable steady states are denoted by green and red, respectively, the blue line is the stability boundary (20), and the dotted blue line is the folding of the surface. In (d), white denotes that no steady state exists, while yellow corresponds to the cases when there are both stable and unstable steady states due to the folding of the surface.

of the cyclic states of the system. Accordingly, when we talk about the stability of the steady-state motions, it is only about the essential dynamics, while the hidden motions may present instability in the Lyapunov sense.

Let us consider two examples when the wheel initially rolls straight along the x-axis. In the first case, a small perturbation may increase the speed of rolling. If the essential states $\omega_1, \omega_2, \omega_3, \vartheta$ remain in the small vicinity of the original values, then the essential motion is stable. However, the increased velocity ω_2 causes the cyclic coordinates φ, x_G to move away linearly in time from the original unperturbed trajectories; therefore, the hidden motion is unstable. In the second case, let the perturbation cause a small tilt angle ϑ_0, tilt rate $\dot{\vartheta}_0 = \omega_{10}$, and/or a small yaw rate $\dot{\psi}_0 = \omega_{30}$. If the essential states remain in the vicinity of the original unperturbed values, then the essential motion is stable. However, this small perturbation yields a circular motion of the wheel with a large radius instead of the straight motion, so the hidden motion is unstable.

For simplicity assume the initial values $\psi_0 = 0$, $\varphi_0 = 0$, $x_0 = 0$, and $y_0 = 0$. According to (5), (8), and (11), the steady-state motion is given as

$$\mathbf{x}_* = \begin{bmatrix} \omega_{1*} \\ \omega_{2*} \\ \omega_{3*} \\ \vartheta_* \\ \dot{\psi}_*(t) \\ \varphi_*(t) \\ x_{G*}(t) \\ y_{G*}(t) \end{bmatrix} = \begin{bmatrix} 0 \\ \dot{\psi}_* \sin\vartheta_* + \dot{\varphi}_* \\ \dot{\psi}_* \cos\vartheta_* \\ \vartheta_* \\ \dot{\psi}_* t \\ \dot{\varphi}_* t \\ \dots \\ \dots \end{bmatrix} \tag{15}$$

where the dots in $x_{G*}(t)$ and $y_{G*}(t)$ refer to (11).

Introducing the state perturbations $\tilde{\mathbf{x}} := \mathbf{x} - \mathbf{x}_*$, (6) leads to the linearized equations of the form $\dot{\tilde{\mathbf{x}}} = \mathrm{A}\tilde{\mathbf{x}}$ where the state matrix is obtained as $\mathrm{A} = f'(\mathbf{x}_*)$. This yields

$$\mathbf{A} = \left[\begin{array}{cccc:cccc} 0 & A_{12} & A_{13} & A_{14} & 0 & 0 & 0 & 0 \\ A_{21} & 0 & 0 & 0 & 0 & 0 & 0 & 0 \\ A_{31} & 0 & 0 & 0 & 0 & 0 & 0 & 0 \\ 1 & 0 & 0 & 0 & 0 & 0 & 0 & 0 \\ \hdashline 0 & 0 & A_{53} & A_{54} & 0 & 0 & 0 & 0 \\ 0 & 1 & A_{63} & A_{64} & 0 & 0 & 0 & 0 \\ A_{71} & A_{72} & 0 & 0 & A_{75} & 0 & 0 & 0 \\ A_{81} & A_{82} & 0 & 0 & A_{85} & 0 & 0 & 0 \end{array}\right] \tag{16}$$

where

$$A_{12} = \frac{6}{5}\dot{\psi}_* \cos\vartheta_*\,, \quad A_{13} = \frac{4}{5}\dot{\psi}_* \sin\vartheta_* + \frac{6}{5}\dot{\varphi}_*\,,$$
$$A_{14} = -\frac{1}{5}\dot{\psi}_*^2 + \frac{4g}{5R}\cos\vartheta_*\,, \quad A_{21} = -\frac{2}{3}\dot{\psi}_* \cos\vartheta_*\,,$$
$$A_{31} = -\dot{\psi}_* \sin\vartheta_* - 2\dot{\varphi}_*\,, \quad A_{53} = \frac{1}{\cos\vartheta_*}\,,$$
$$A_{54} = \dot{\psi}_* \tan\vartheta_*\,, \quad A_{63} = -\tan\vartheta_*\,,$$
$$A_{64} = -\frac{\dot{\psi}_*}{\cos\vartheta_*}\,, \quad A_{71} = R\sin\psi_*\cos\vartheta_*\,,$$
$$A_{72} = R\cos\psi_*\,, \quad A_{75} = -R\sin\psi_*\left(\dot{\psi}_*\sin\vartheta_* + \dot{\varphi}_*\right),$$
$$A_{81} = -R\cos\psi_*\cos\vartheta_*\,, \quad A_{82} = R\sin\psi_*\,,$$
$$A_{85} = R\cos\psi_*\left(\dot{\psi}_*\sin\vartheta_* + \dot{\varphi}_*\right)\,, \tag{17}$$

and the pitch rate $\dot{\varphi}_*$ must be substituted according to (12). The dashed lines distinguish the parts of $\mathbf{A}$ related to the essential and the hidden dynamics.

The linear stability of the steady-state (essential) motion can be determined by the characteristic equation $\det(\lambda\mathbf{I} - \hat{\mathrm{A}}) = 0$, where $\hat{\mathrm{A}}$ is the top quadrant of $\mathbf{A}$ in (16). This yields

$$\left(\lambda^2 - A_{12}A_{21} - A_{13}A_{31} - A_{14}\right)\lambda^2 = 0\,, \tag{18}$$

and the characteristic roots become

$$\lambda_{1,2} = \pm\sqrt{\frac{4g}{5R}\cos\vartheta_* - \left(\dot{\psi}_*^2 + \frac{14}{5}\dot{\psi}_*\dot{\varphi}_*\sin\vartheta_* + \frac{12}{5}\dot{\varphi}_*^2\right)},$$
$$\lambda_{3,4} = 0. \tag{19}$$

The corresponding steady state is unstable if the characteristic roots are real, $\lambda_{1,2} \in \mathbb{R}$ and $\lambda_1 = -\lambda_2$. Otherwise, if the first two characteristic roots constitute a purely imaginary complex conjugate pair $\lambda_{1,2} \in \mathbb{C}$ and $\lambda_1 = \bar{\lambda}_2$, a "doubtful Lyapunov" case arises due to the zero eigenvalue of multiplicity two. One may show, however, that both the algebraic and geometric multiplicity of the zero eigenvalue are two, and in Appendix B, the Lyapunov stability of the essential dynamics is proved. Note that the full motion is not stable in the Lyapunov sense due to the zero eigenvalue of algebraic multiplicity four and geometric multiplicity one belonging to the hidden dynamics [see the lower right quadrant of state matrix (16)].

To sum up the analysis of the linear model, the necessary and sufficient condition for the stable rolling of the wheel is

$$\dot{\psi}_*^2 + \frac{14}{5}\dot{\psi}_*\dot{\varphi}_*\sin\vartheta_* + \frac{12}{5}\dot{\varphi}_*^2 - \frac{4g}{5R}\cos\vartheta_* > 0\,, \tag{20}$$

where (12) holds. When varying the tilt angle ϑ_*, the yaw rate $\dot{\psi}_*$ and pitch rate $\dot{\varphi}_*$, one may change the stability of the steady-state motion.

1) Turning-Rolling: In the case of a general turning-rolling-type steady-state motion, neither the tilt angle nor the yaw and pitch rates are zero, that is, $\vartheta_* \neq 0$, $\dot{\psi}_* \neq 0$, and $\dot{\varphi}_* \neq 0$. Then, the stability of the steady-state changes at the critical yaw rates

$$\dot{\psi}_{\mathrm{crit},1,2} = \sqrt{\frac{2g}{5R}}\sqrt{\frac{3 - 6\cos^2\vartheta_* \pm \sqrt{76\sin^4\vartheta_* - 96\sin^2\vartheta_* + 9}}{\left(2\sin^2\vartheta_* - 3\right)\cos\vartheta_*}} \tag{21}$$

for

$$|\vartheta_*| \leq \mathcal{V} = \arcsin\left(\sqrt{\tfrac{12}{19} - \tfrac{9\sqrt{5}}{38}}\right) \approx 18.62^\circ. \tag{22}$$

For a given tilt angle $|\vartheta_*| \leq \mathcal{V}$, if $|\dot{\psi}_*| < \dot{\psi}_{\mathrm{crit},1}$ or $\dot{\psi}_{\mathrm{crit},2} < |\dot{\psi}_*|$, then the characteristic roots in (19) are purely imaginary $\lambda_{1,2} \in \mathbb{C}$ and $\lambda_1 = \bar{\lambda}_2$ and the corresponding motion is stable. Otherwise, if $\dot{\psi}_{\mathrm{crit},1} < |\dot{\psi}_*| < \dot{\psi}_{\mathrm{crit},2}$, then the characteristic roots are real $\lambda_{1,2} \in \mathbb{R}$ and $\lambda_1 = -\lambda_2$, and the corresponding motion is unstable. Notice that, if the tilt angle is large enough $|\vartheta_*| > \mathcal{V}$, then all corresponding steady-state motions are stable, since $\mathcal{V}$ is independent of any physical parameter. This is a fundamental physical constant related to the steady-state stability of any rolling wheel.

2) Straight Rolling: As discussed above, the straight rolling steady-state motion ($\dot{\psi}_* = 0$) can only occur for zero tilt angle $\vartheta_* = 0$. That is, the steady-state (15) simplifies to

$$\omega_{2*} = \dot{\varphi}_*\,, \quad \varphi_*(t) = \dot{\varphi}_* t\,, \quad x_{\mathrm{G}*}(t) = R\dot{\varphi}_* t\,, \tag{23}$$

and all the other states become zero. The state matrix (16) is

$$\mathbf{A} = \left[\begin{array}{cccc:cccc} 0 & 0 & \frac{6}{5}\dot{\varphi}_* & \frac{4g}{5R} & 0 & 0 & 0 & 0 \\ 0 & 0 & 0 & 0 & 0 & 0 & 0 & 0 \\ -2\dot{\varphi}_* & 0 & 0 & 0 & 0 & 0 & 0 & 0 \\ 1 & 0 & 0 & 0 & 0 & 0 & 0 & 0 \\ \hdashline 0 & 0 & 1 & 0 & 0 & 0 & 0 & 0 \\ 0 & 1 & 0 & 0 & 0 & 0 & 0 & 0 \\ 0 & R & 0 & 0 & 0 & 0 & 0 & 0 \\ -R & 0 & 0 & 0 & R\dot{\varphi}_* & 0 & 0 & 0 \end{array}\right] \tag{24}$$

and the characteristic roots (19) simplify to

$$\lambda_{1,2} = \pm\sqrt{\frac{4g}{5R} - \frac{12}{5}\dot{\varphi}_*^2}\,. \tag{25}$$

This leads to the critical pitch rate

$$\dot{\varphi}_{\mathrm{crit}} = \sqrt{\frac{g}{3R}}\,, \tag{26}$$

that is, the straight rolling steady state is stable if the wheel rolls fast enough, $|\dot{\varphi}_*| > \dot{\varphi}_{\mathrm{crit}}$. Otherwise, it is unstable.

We remark that instead of the pitch rate $\dot{\varphi}_*$, one may introduce the parameter $v_* = \dot{\varphi}_* R$, which is the steady-state velocity of the center of gravity. This way, the critical pitch rate (26) can be converted to a critical velocity.

3) Spinning on the Spot: The spinning steady-state motion ($\dot{\varphi}_* = 0$) can also occur for zero tilt angle $\vartheta_* = 0$. Then, the steady state becomes

$$\omega_{3*} = \dot{\psi}_*\,, \quad \psi_* = \dot{\psi}_* t\,, \tag{27}$$

and all the other states are zero. The state matrix (16) becomes

$$\mathbf{A} = \left[\begin{array}{cccc:cccc} 0 & \frac{6}{5}\dot{\psi}_* & 0 & \frac{4g}{5R} - \frac{1}{5}\dot{\psi}_*^2 & 0 & 0 & 0 & 0 \\ -\frac{2}{3}\dot{\psi}_* & 0 & 0 & 0 & 0 & 0 & 0 & 0 \\ 0 & 0 & 0 & 0 & 0 & 0 & 0 & 0 \\ 1 & 0 & 0 & 0 & 0 & 0 & 0 & 0 \\ \hdashline 0 & 0 & 1 & 0 & 0 & 0 & 0 & 0 \\ 0 & 1 & 0 & -\dot{\psi}_* & 0 & 0 & 0 & 0 \\ R\sin\psi_* & R\cos\psi_* & 0 & 0 & 0 & 0 & 0 & 0 \\ -R\cos\psi_* & R\sin\psi_* & 0 & 0 & 0 & 0 & 0 & 0 \end{array}\right] \tag{28}$$

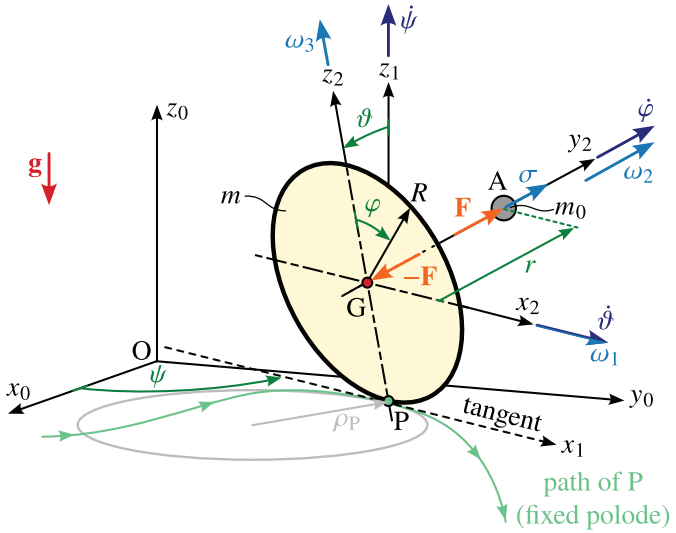

Fig. 4. Model of the unicycle for maneuvering.

while the characteristic roots (19) and the critical yaw rate (21) simplify to

$$\lambda_{1,2} = \pm\sqrt{\frac{4g}{5R} - \dot\psi_*^2}\,, \qquad \dot\psi_{\text{crit}} = \sqrt{\frac{4g}{5R}}\,. \tag{29}$$

That is, the spinning steady state is stable if the wheel spins fast enough $|\dot\psi_*| > \dot\psi_{\text{crit}}$. Otherwise, it is unstable.

All results about the steady-state motions and their stability are shown in Fig. 3. Fig. 3(a) shows the steady-state motions (12) as surface in the $(\vartheta_*, \dot\psi_*, \dot\varphi_*)$ space. Fig. 3(b) shows the level sets of ϑ_* in the $(\dot\psi_*, \dot\varphi_*)$ plane. Similarly, Fig. 3(c) and (d) shows the level sets of $\dot\psi_*$ and $\dot\varphi_*$, respectively. Green (▬) and red (▬) areas represent stable and unstable steady-state solutions, respectively, while the blue solid line (—) is the stability boundary (20). The dashed blue line (– –) in Fig. 3(c) shows where $\dot\varphi_* \to \pm\infty$. The dotted blue curves (···) in Fig. 3(b) and (c) indicate the folding of the surface, and these bound the hourglass-shaped area in Fig. 3(d). In the dark green area (▬) in Fig. 3(d), two stable steady states exist with different yaw rates $\dot\psi_*$, while in the yellow area (▬), a stable and an unstable steady state exist. In the white area, no steady state exists regardless of the yaw rate due to the folding of the surface.

III. Modeling the Unicycle

The unicycle is shown in Fig. 4, where the motion is controlled by moving a mass point along the axle of the wheel. In this section, we present the governing equations and analyze the steady states of the open-loop system.

A. Governing Equations

The model of the unicycle is built upon the rolling wheel model presented in Section II with the added point mass m_0 moving along the axle. The relative position of the mass is given by

$$\mathbf{r}_{\text{GA}} = \begin{bmatrix} 0 & r & 0 \end{bmatrix}^\top_{\text{F}_2}\,, \tag{30}$$

where r represents the position of the point mass along the axle, while the other two coordinates are constrained at zero by the axle, resulting in two geometric constraints. Between the disk and the point mass, there is an internal pair of forces; the control force acting on the point mass is

$$\mathbf{F} = \begin{bmatrix} 0 & u & 0 \end{bmatrix}^\top_{\text{F}_2}\,, \tag{31}$$

while $-\mathbf{F}$ acts on the wheel with opposite sense. The control input u is used for balancing and steering the unicycle.

The equations of motion of the unicycle are derived in Appendix C in a similar way as for the rolling wheel; the differences between the two models are highlighted below. The rolling constraints of the wheel still hold, yielding two kinematic constraints (2) and one geometric constraint (3). Thus, the unicycle is a nonholonomic mechanical system with $n_{\text{g}} = 3$ geometric constraints and $n_{\text{k}} = 2$ kinematic constraints. Accordingly, $n_q = 9 - n_{\text{g}} = 6$ generalized coordinates have to be chosen to describe the system unambiguously; let these be

$$(x_{\text{G}},\ y_{\text{G}},\ \vartheta,\ \psi,\ \varphi,\ r)\,. \tag{32}$$

Moreover, $n_\sigma = n_q - n_{\text{k}} = 4$ pseudovelocities have to be chosen; let these be the components of the angular velocity $\boldsymbol{\omega}$ of the wheel (see (73) in Appendix C) and the axle directional velocity component of the point mass

$$\begin{aligned} &\omega_1(t) := \dot\vartheta, && \omega_2(t) := \dot\psi\sin\vartheta + \dot\varphi\,,\\ &\omega_3(t) := \dot\psi\cos\vartheta, && \sigma(t) := \dot r - \dot\vartheta R\,. \end{aligned} \tag{33}$$

The Appellian approach yields the equations of motion

$$\begin{cases} \dot\omega_1 = \dfrac{1}{5mR^2+4m_0r^2}\Big(-4\omega_1^2 m_0 Rr - \omega_3^2\big(mR^2+4m_0r^2\big)\tan\vartheta \\ \qquad -8\omega_1\sigma m_0 r + \omega_2\omega_3\big(6mR^2+4m_0Rr\tan\vartheta\big) \\ \qquad -4m_0 gr\cos\vartheta + 4mgR\sin\vartheta + 4Ru\Big)\,, \\ \dot\omega_2 = \dfrac{2}{3mR^2+2m_0R^2+12m_0r^2}\Big(-2\omega_1\omega_2 m_0 Rr \\ \qquad +\omega_1\omega_3\big(m_0R^2 - mR^2 - 4m_0r^2\big) + 2\omega_3\sigma m_0 R\Big)\,, \\ \dot\omega_3 = \dfrac{1}{3mR^2+2m_0R^2+12m_0r^2}\Big(-\omega_1\omega_2\big(6mR^2+4m_0R^2\big) \\ \qquad +\omega_1\omega_3\big(\big(3mR^2+2m_0R^2+12m_0r^2\big)\tan\vartheta\big) \\ \qquad -24\omega_3\sigma m_0 r - 20m_0Rr\Big)\,, \\ \dot\vartheta = \omega_1\,, \\ \dot\sigma = \omega_1^2 r + \omega_3^2 r - \omega_2\omega_3 R - g\sin\vartheta + \dfrac{1}{m_0}u\,, \\ \dot r = \sigma + \omega_1 R\,, \end{cases}$$

$$\begin{cases} \dot\psi = \omega_3\dfrac{1}{\cos\vartheta}\,, \\ \dot\varphi = \omega_2 - \omega_3\tan\vartheta\,, \\ \dot x_{\text{G}} = \omega_1 R\sin\psi\cos\vartheta + \omega_2 R\cos\psi\,, \\ \dot y_{\text{G}} = -\omega_1 R\cos\psi\cos\vartheta + \omega_2 R\sin\psi\,, \end{cases} \tag{34}$$

which is a $n = 9 - n_{\text{g}} - n_{\text{k}}/2 = 5$DoF nonholonomic mechanical system. The equations of motion (34) of the unicycle can be divided into essential dynamics (first six equations) and hidden dynamics (remaining four equations) [22]. Observe that the hidden dynamics of the unicycle (34) are identical to that of the rolling wheel (6). Moreover, considering $m_0 = 0$ and $u = 0$, the essential dynamics in (34) simplify to that in

(6). The dynamical model (34) of the unicycle is formulated as a control affine system $\dot{\mathbf{x}} = f(\mathbf{x}) + g(\mathbf{x})u$ with the state vector

$$\mathbf{x} = \left[\begin{array}{cccccc|cccc} \omega_1 & \omega_2 & \omega_3 & \vartheta & \sigma & r & \psi & \varphi & x_G & y_G \end{array}\right]^\top, \tag{35}$$

and control input u; so, this model is ready for control design.

B. Steady States

Considering $u \equiv 0$ (i.e., the point mass freely moves along the axle), the unicycle model (34) possesses the steady-state motion with essential dynamics

$$\begin{aligned} &\omega_1(t) \equiv \omega_{1*}, \quad \omega_2(t) \equiv \omega_{2*}, \quad \omega_3(t) \equiv \omega_{3*}, \\ &\vartheta(t) \equiv \vartheta_*, \quad \sigma(t) \equiv \sigma_*, \quad r(t) \equiv r_*. \end{aligned} \tag{36}$$

Substituting this into the first six equations of (34) yields

$$\begin{aligned} &\omega_{2*}\omega_{3*}\left(6mR^2 + 4m_0Rr_*\tan\vartheta_*\right) - 4m_0gr_*\cos\vartheta_* \\ &\quad - \omega_{3*}^2\left(mR^2 + 4m_0r_*^2\right)\tan\vartheta_* + 4mgR\sin\vartheta_* = 0, \\ &\omega_{3*}^2 r_* - \omega_{2*}\omega_{3*}R - g\sin\vartheta_* = 0, \end{aligned} \tag{37}$$

while the hidden motion of the unicycle is the same as the hidden motion of the rolling wheel described in (10) and (11).

Using (33), the relations (37) can be reformulated using the generalized velocities $(\dot{\psi}_*, \dot{\vartheta}_*, \dot{\varphi}_*, \dot{r}_*)$

$$\begin{aligned} &\dot{\psi}_*^2\left(4m_0Rr_*\sin^2\vartheta_* + \left(5mR^2 - 4m_0r_*^2\right)\sin\vartheta_*\cos\vartheta_*\right) \\ &\quad + \dot{\psi}_*\dot{\varphi}_*\left(6mR^2\cos\vartheta_* + 4m_0Rr_*\sin\vartheta_*\right) \\ &\quad - 4m_0gr_*\cos\vartheta_* + mgR\sin\vartheta_* = 0, \\ &\dot{\psi}_*^2\left(r_*\cos^2\vartheta_* - R\sin\vartheta_*\cos\vartheta_*\right) \\ &\quad - \dot{\psi}_*\dot{\varphi}_*R\cos\vartheta_* - g\sin\vartheta_* = 0. \end{aligned} \tag{38}$$

Then, one may express the pitch rate $\dot{\varphi}_*$ and point mass position r_* as a function of the tilt angle ϑ_* and the yaw rate $\dot{\psi}_*$

$$\begin{aligned} \dot{\varphi}_* &= \frac{\tan\vartheta_*}{\dot{\psi}_*R\left(6\dot{\psi}_*^2mR\cos^3\vartheta_* - 4m_0g\right)} \\ &\quad \cdot\left(-5\dot{\psi}_*^4mR^2\cos^4\vartheta_* + 4\dot{\psi}_*^2gR\left(m_0\cos\vartheta_* - m\cos^3\vartheta_*\right)\right. \\ &\qquad \left. + 4m_0g^2\right), \\ r_* &= \frac{mR\left(\dot{\psi}_*^2R\cos\vartheta_* + 2\,g\right)\sin\vartheta_*\cos\vartheta_*}{6\dot{\psi}_*^2mR\cos^3\vartheta_* - 4m_0g}, \end{aligned} \tag{39}$$

if

$$\dot{\psi}_* \neq 0, \quad \dot{\psi}_* \neq \pm\sqrt{\frac{2m_0g}{3mR\cos^3\vartheta_*}} \tag{40}$$

holds. For the nongeneric cases, when (40) does not hold, the steady-state motions are explained below.

When the yaw rate is zero $\dot{\psi}_* = 0$, straight rolling occurs and (38) simplify to

$$4mR\sin\vartheta_* - 4m_0r_*\cos\vartheta_* = 0, \quad g\sin\vartheta_* = 0. \tag{41}$$

These are only satisfied for zero tilt angle $\vartheta_* = 0$ and centered point mass $r_* = 0$, independent of the pitch rate $\dot{\varphi}_*$.

In the case of $\dot{\psi}_* = \pm(2m_0g/(3mR\cos^3\vartheta_*))^{1/2}$, (38) still results in zero tilt angle $\vartheta_* = 0$ and

$$\dot{\psi}_{*1,2} = \pm\sqrt{\frac{2m_0g}{3mR}}, \quad \dot{\varphi}_{*1,2} = \pm\sqrt{\frac{2m_0g}{3mR^3}}r_*, \tag{42}$$

which describes a turning-rolling steady-state motion with a nontilted wheel. This is a new behavior of the unicycle which does not exist for a rolling wheel, as the latter must be tilted to have a turning-rolling steady-state motion [see (12)]. Note that, this steady state can only occur for the specific yaw rates $\dot{\psi}_{*1,2}$ depending only on physical parameters, while the corresponding pitch rates $\dot{\varphi}_{*1,2}$ also depend only on the point mass position r_*. The nontilted turning steady state becomes a spinning steady state ($\dot{\varphi}_{*1,2} = 0$) if the point mass is at the center $r_* = 0$.

The other spinning steady state can be obtained by substituting zero pitch rate $\dot{\varphi}_* = 0$ into (38), which yields

$$\begin{aligned} &\dot{\psi}_*^2\left(\left(5mR^2 - 4m_0r_*^2\right)\sin\vartheta_*\cos\vartheta_* + 4m_0Rr_*\sin^2\vartheta_*\right) \\ &\quad + 4mgR\sin\vartheta_* - 4m_0gr_*\cos\vartheta_* = 0, \\ &\dot{\psi}_*^2\left(r_*\cos^2\vartheta_* - R\sin\vartheta_*\cos\vartheta_*\right) - g\sin\vartheta_* = 0. \end{aligned} \tag{43}$$

Similar to the spinning wheel, such steady-state motion exists for zero tilt angle ($\vartheta_* = 0$) when the point mass is at the center $r_* = 0$. However, in the case of the unicycle, spinning type steady-state motion also exists with nonzero tilt angle ($\vartheta_* \neq 0$) when

$$\begin{aligned} \dot{\psi}_* &= \pm\sqrt{\frac{4m_0gr_*\cos\vartheta_* - 4mgR\sin\vartheta_*}{\left(5mR^2 - 4m_0r_*^2\right)\sin\vartheta_*\cos\vartheta_* + 4m_0Rr_*\sin^2\vartheta_*}}, \\ r_* &= \frac{R\tan\vartheta_*}{2m_0}\left(m\cos^2\vartheta_* + m_0\right. \\ &\qquad \left. + \sqrt{m^2\cos^4\vartheta_* + 3mm_0\cos^2\vartheta_* + m_0^2}\right). \end{aligned} \tag{44}$$

We refer to this as tilted spinning, which is also a new behavior of the unicycle compared to the rolling wheel. According to (44), the point mass is always above the wheel center since $\operatorname{sgn} r_* = \operatorname{sgn}\vartheta_*$ or $r_*\vartheta_* > 0$ (see Fig. 4). Investigating special cases like $\vartheta_* = 0$ or $r_* = 0$ leads to steady states already discussed above.

One limiting factor of our unicycle model is that the point mass may slide below the ground, which is physically not feasible. To exclude these cases, one can calculate the z coordinate of the position vector $\mathbf{r}_A = \mathbf{r}_G + \mathbf{r}_{GA}$ in frame F_0 and require it to be positive. This yields $R\cos\vartheta_* + r_*\sin\vartheta_* > 0$.

All steady-state motions of the unicycle are summarized in Fig. 5 in the plane of the steady-state tilt angle ϑ_* and the yaw rate $\dot{\psi}_*$. The straight rolling, that is, $\vartheta_* = 0$ and $\dot{\psi}_* = 0$, is marked by a black square ■; in this case, the steady-state pitch rate $\dot{\varphi}_*$ may be arbitrary, and the point mass is at wheel center $r_* = 0$. The nontilted turning, that is, $\vartheta_* = 0$ and $\dot{\psi}_* = \dot{\psi}_{*1,2}$, is marked by black dots •; in this case, the pitch rate $\dot{\varphi}_*$ and the point mass position r_* linked as in (42). The regular (nontilted) spinning steady-state motions, that is, $\vartheta_* = 0$ and $\dot{\varphi}_* = 0$, are shown by the solid black line (—); in this case, the yaw rate $\dot{\psi}_*$ may be arbitrary, and the point mass is at the wheel center $r_* = 0$. The tilted spinning steady states, that is, $\dot{\varphi}_* = 0$ and $\vartheta_* \neq 0$, are shown by dashed black lines (– –); the corresponding yaw rate $\dot{\psi}_*$ and point mass position r_* are expressed by (44). The general turning-rolling steady states are divided into separate areas. The light blue and light purple areas show the physically feasible steady states when the point mass is placed below $0 < z_A < z_G$ or above

$z_A > z_G$ the wheel center point G, respectively. The white area ▭ represents the physically unfeasible steady states when the point mass is at or below the ground level, that is, $z_A \leq 0$.

Note that Fig. 5 was constructed using the numerical parameters in Table I. Using different parameters, like different mass ratios m_0/m, the main structure of the steady states remains qualitatively similar, but the shape and size of the parameter regions related to the nonfeasible steady states may be different.

The steady states have been categorized by considering zero input force ($u \equiv 0$). Assuming a nonzero constant input ($u \equiv u_*$) may result in further steady states. For example, a straight rolling case may occur with a tilted wheel when the mass is held 'above' the wheel center. Studying such steady states is out of the scope of the present study.

C. Stability of Steady States

Linear stability analysis is performed to determine the stability of the previously discussed steady-state motions of the unicycle. Linearizing (34) around a steady state $\mathbf{x}_*$ leads to the form $\dot{\tilde{\mathbf{x}}} = A\tilde{\mathbf{x}}$ where $\tilde{\mathbf{x}} = \mathbf{x} - \mathbf{x}_*$ denotes the perturbed states and state matrix $A = f'(\mathbf{x}_*)$ can be written as (45), shown at the bottom of the page,whose elements are given in Appendix D. Note that the steady-state tilt angle ϑ_*, yaw rate $\dot{\psi}_*$, pitch rate $\dot{\varphi}_*$, and point mass position r_* in the elements of $\mathbf{A}$ are not independent of each other, they must satisfy (38). Therefore, each of the different steady-state motions (turning-rolling, straight rolling, and nontilted turning) must be analyzed separately. In this article, we focus on the straight rolling and turning-rolling motions while the nontilted turning is left for future research. Also note that the spinning steady state is a special case of the more general turning-rolling steady state; since it has minor practical relevance, its further analysis is omitted.

The characteristic equation $\det(\lambda\mathbf{I} - \hat{A}) = 0$, where $\hat{A}$ is the top left 6×6 part of $\mathbf{A}$ in (45), takes the form

$$\begin{aligned}\big(\lambda^4 - \lambda^2 (&A_{12}A_{21} + A_{13}A_{31} + A_{14} + A_{16}A_{61} + A_{25}A_{52} \\ &+ A_{35}A_{53} + A_{56}) + A_{12}A_{21}A_{35}A_{53} - A_{12}A_{25}A_{31}A_{53} \\ &- A_{12}A_{25}A_{56}A_{61} - A_{13}A_{21}A_{35}A_{52} + A_{13}A_{25}A_{31}A_{52} \\ &- A_{13}A_{35}A_{56}A_{61} + A_{16}A_{25}A_{52}A_{61} + A_{16}A_{35}A_{53}A_{61} \\ &+ A_{12}A_{21}A_{56} - A_{12}A_{25}A_{54} + A_{13}A_{31}A_{56} - A_{13}A_{35}A_{54} \\ &+ A_{14}A_{25}A_{52} + A_{14}A_{35}A_{53} - A_{16}A_{21}A_{52} - A_{16}A_{31}A_{53} \\ &+ A_{14}A_{56} - A_{16}A_{54}\big)\lambda^2 = 0\,. \end{aligned} \tag{46}$$

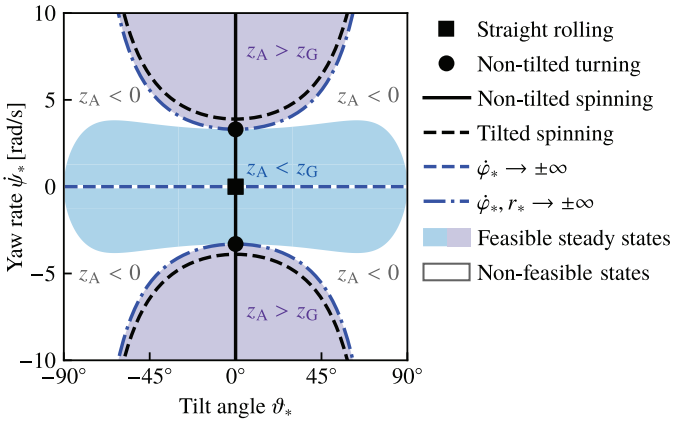

Fig. 5. Summary of the steady-state motions of the unicycle.

TABLE I
NUMERICAL PARAMETERS FOR THE ROLLING WHEEL AND UNICYCLE

Quantity	Symbol	Value	Unit
wheel mass	m	10	kg
point mass	m_0	5	kg
wheel radius	R	0.3	m
gravitational acceleration	g	9.81	m/s^2

1) Turning-Rolling Steady State: When calculating the characteristic roots of (46), the steady-state pitch rate $\dot{\varphi}_*$ and point mass position r_* must be substituted according to (39). Due to the highly complicated expressions, numerical evaluation is used to obtain the characteristic roots and determine the stability of the turning-rolling steady states. The results are shown in Fig. 6 for several mass ratios with $m_0 = 0, 1, 2, 5, 10, 15, 20, 30$ kg, while the other physical parameters are presented in Table I. The same coloring scheme is used as in Fig. 3, namely, green (▬) and red (▬) areas represent stable and unstable steady-state solutions, respectively, while the white area (▭) represents the physically unfeasible steady states with point mass at or below the ground level (see Fig. 5). The case with $m_0 = 0$ is identical to the rolling wheel in Fig. 3(c). By the addition of the point mass $m_0 > 0$, the stability properties change drastically since the number of DoF is increased, additional types of equilibria are born (the tilted spinning and the vertical turning), the point mass may be above or below the wheel, and it even may hit the ground, as was discussed in Section III-B and Fig. 5.

$$A = \left[\begin{array}{cccccc:cccc} 0 & A_{12} & A_{13} & A_{14} & 0 & A_{16} & 0 & 0 & 0 & 0 \\ A_{21} & 0 & 0 & 0 & A_{25} & 0 & 0 & 0 & 0 & 0 \\ A_{31} & 0 & 0 & 0 & A_{35} & 0 & 0 & 0 & 0 & 0 \\ 1 & 0 & 0 & 0 & 0 & 0 & 0 & 0 & 0 & 0 \\ 0 & A_{52} & A_{53} & A_{54} & 0 & A_{56} & 0 & 0 & 0 & 0 \\ A_{61} & 0 & 0 & 0 & 1 & 0 & 0 & 0 & 0 & 0 \\ \hdashline 0 & 0 & A_{73} & A_{74} & 0 & 0 & 0 & 0 & 0 & 0 \\ 0 & 1 & A_{83} & A_{84} & 0 & 0 & 0 & 0 & 0 & 0 \\ A_{91} & A_{92} & 0 & 0 & 0 & 0 & A_{97} & 0 & 0 & 0 \\ A_{101} & A_{102} & 0 & 0 & 0 & 0 & A_{107} & 0 & 0 & 0 \end{array}\right] \tag{45}$$

With small point masses (such as $m_0 = 1, 2$ kg), the vertical spinning ($\vartheta_* = 0$) becomes unstable as the point mass is pushed away from the spinning wheel by the centrifugal force. With large point masses (such as $m_0 = 15, 20, 30$ kg), a stable yaw rate $\dot{\psi}_*$ band appears, but the spinning steady states remain unstable for large enough yaw rates.

2) Straight Rolling: The steady state is given as (23) and all the other states become zero, considering that the initial values x_0, y_0, and $\dot{\psi}_0$ are zeros. The state matrix (45) simplifies to

$$\mathbf{A} = \left[\begin{array}{cccccc|cccc} 0 & 0 & \frac{6}{5}\dot{\varphi}_* & \frac{4g}{5R} & 0 & -\frac{4m_0 g}{5mR^2} & 0 & 0 & 0 & 0 \\ 0 & 0 & 0 & 0 & 0 & 0 & 0 & 0 & 0 & 0 \\ -2\dot{\varphi}_* & 0 & 0 & 0 & 0 & 0 & 0 & 0 & 0 & 0 \\ 1 & 0 & 0 & 0 & 0 & 0 & 0 & 0 & 0 & 0 \\ 0 & 0 & -R\dot{\varphi}_* & -g & 0 & 0 & 0 & 0 & 0 & 0 \\ R & 0 & 0 & 0 & 1 & 0 & 0 & 0 & 0 & 0 \\ \hline 0 & 0 & 1 & 0 & 0 & 0 & 0 & 0 & 0 & 0 \\ 0 & 1 & 0 & 0 & 0 & 0 & 0 & 0 & 0 & 0 \\ 0 & R & 0 & 0 & 0 & 0 & 0 & 0 & 0 & 0 \\ -R & 0 & 0 & 0 & 0 & 0 & R\dot{\varphi}_* & 0 & 0 & 0 \end{array}\right]. \tag{47}$$

When comparing this with (24) obtained for the rolling wheel, there are two extra rows and columns, 5 and 6, related to the new states r and σ_4.

The characteristic polynomial (46) reduces to

$$\left(a\lambda^4 + b\lambda^2 + c\right)\lambda^2 = 0\,, \tag{48}$$

where

$$\begin{aligned} a &= 5mR^2\,, \\ b &= 12\dot{\varphi}_*^2 mR^2 + 4\,(m_0 - m)\,gR\,, \\ c &= 4m_0 g\left(2\dot{\varphi}_*^2 R - g\right)\,. \end{aligned} \tag{49}$$

Applying the same arguments as in Appendix B, the straight rolling is said to be stable if the coefficients a, b, and c have the same signs. While $a > 0$ always holds, $b > 0$ and $c > 0$ lead to

$$|\dot{\varphi}_*| > \sqrt{\frac{(m - m_0)\,g}{3mR}} \quad \text{and} \quad |\dot{\varphi}_*| > \sqrt{\frac{g}{2R}}\,, \tag{50}$$

respectively. The second condition is always stronger, so the critical pitch rate of the unicycle is

$$\dot{\varphi}_{\text{crit}} = \sqrt{\frac{g}{2R}}\,. \tag{51}$$

That is, the straight rolling of the uncontrolled unicycle is stable if $|\dot{\varphi}_*| > \dot{\varphi}_{\text{crit}}$; it is unstable if $|\dot{\varphi}_*| < \dot{\varphi}_{\text{crit}}$.

Note that, the critical pitch rate (51) is independent of the masses m and m_0. Also, it is larger than the critical pitch rate of the rolling disk (26). The dependency of the characteristic roots on the steady-state pitch rate $\dot{\varphi}_*$ are summarized in Fig. 7 for both the rolling wheel ($m_0 = 0$) and the unicycle ($m_0 > 0$). Observe that in the case of the rolling wheel, the characteristic roots $\lambda_{1,2}$ (thick gray curves) determine the criticality. Contrarily, in the case of the unicycle (even for small values of m_0!), the criticality is determined by the characteristic roots $\lambda_{3,4}$ (orange curves) rather than by the characteristic roots $\lambda_{1,2}$ (blue curves). This resolves the seemingly contradictory issue that the critical pitch rate "jumps" from (26) to (51) when m_0 becomes positive. On the other hand, this is not surprising in view of the different DoFs in the two systems.

3) Spinning on the Spot: The stability analysis of this steady state is covered by the analysis of the turning-rolling motion. Since the motion has minor practical relevance for unicycles, further discussions are omitted here.

IV. Steering Control of the Unicycle

The straight rolling steady state (23) is used as the basis for designing the steering controller of the unicycle. For simplicity, it is assumed that the unicycle has an initial pitch rate $\dot{\varphi}_0 = \dot{\varphi}_*$ and initially it travels along the x_0-axis. Above, we showed that the straight rolling steady state might be unstable or stable without control. Here, we demonstrate that this motion can be made asymptotically stable with appropriate feedback control.

The linear state-space model of the unicycle assumes the form $\dot{\tilde{\mathbf{x}}} = \mathrm{A}\tilde{\mathbf{x}} + \mathbf{B}u$ where $\tilde{\mathbf{x}} = \mathbf{x} - \mathbf{x}_*$. The state matrix $\mathrm{A} = f'(\mathbf{x}_*)$ is given in (47) and it depends on the steady-state pitch rate $\dot{\varphi}_*$. The input matrix $\mathbf{B} = g(\mathbf{x}_*)$ is given by

$$\mathbf{B} = \left[\tfrac{4}{5mR} \;\; 0 \;\; 0 \;\; 0 \;\; \tfrac{1}{m_0} \;\; 0 \;\; 0 \;\; 0 \;\; 0 \;\; 0\right]^\top. \tag{52}$$

A. Controllability

The controllability matrix of the unicycle is obtained as

$$\mathbf{M}_c = \left[\mathbf{B} \;\; \mathbf{AB} \;\; \mathbf{A}^2\mathbf{B} \;\; \ldots \;\; \mathbf{A}^9\mathbf{B}\right]. \tag{53}$$

Substituting (47) and (52), we obtain (54), as shown at the bottom of the page, with $c = -2\dot{\varphi}_*$. Notice that rows 2, 8, and 9 are full of zeros while rows 3 and 4 are linearly dependent.

$$\mathbf{M}_c = \begin{bmatrix} M_{11} & 0 & M_{13} & 0 & M_{15} & 0 & M_{17} & 0 & M_{19} & 0 \\ 0 & 0 & 0 & 0 & 0 & 0 & 0 & 0 & 0 & 0 \\ 0 & cM_{42} & 0 & cM_{44} & 0 & cM_{46} & 0 & cM_{48} & 0 & cM_{410} \\ 0 & M_{42} & 0 & M_{44} & 0 & M_{46} & 0 & M_{48} & 0 & M_{410} \\ M_{51} & 0 & M_{53} & 0 & M_{55} & 0 & M_{57} & 0 & M_{59} & 0 \\ 0 & M_{62} & 0 & M_{64} & 0 & M_{66} & 0 & M_{68} & 0 & M_{610} \\ 0 & 0 & M_{73} & 0 & M_{75} & 0 & M_{77} & 0 & M_{79} & 0 \\ 0 & 0 & 0 & 0 & 0 & 0 & 0 & 0 & 0 & 0 \\ 0 & 0 & 0 & 0 & 0 & 0 & 0 & 0 & 0 & 0 \\ 0 & M_{102} & 0 & M_{104} & 0 & M_{106} & 0 & M_{108} & 0 & M_{1010} \end{bmatrix} \tag{54}$$

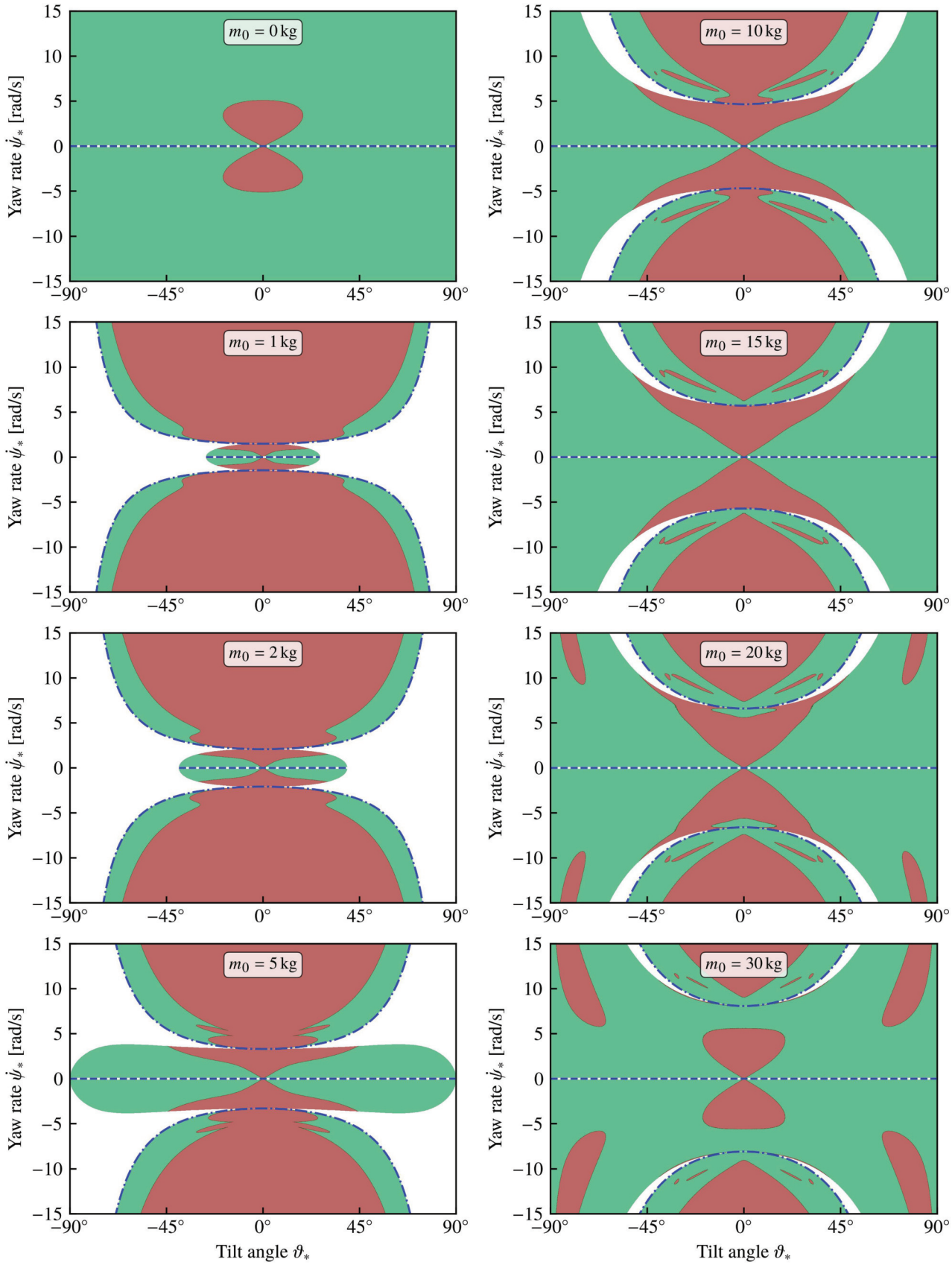

Fig. 6. Stability of steady-state motions of the unicycle for various m_0 values: stable and unstable steady states are denoted by green and red, respectively, while white denotes the unfeasible steady states when the point mass hits the ground.

Thus, $\operatorname{rank}\mathbf{M}_c = 6$ and the controllability matrix is not full row rank. That is, at the linear level, the unicycle is not fully controllable with the single input u.

When spelling out the third and fourth equations in the linear system $\dot{\tilde{\mathbf{x}}} = \mathrm{A}\tilde{\mathbf{x}} + \mathbf{B}u$, one obtains

$$\dot{\omega}_3 = -2\dot{\varphi}_*\omega_1\,, \quad \dot{\vartheta} = \omega_1 \tag{55}$$

which leads to

$$\omega_3 = -2\dot{\varphi}_*\vartheta. \tag{56}$$

This means that the yaw rate $\dot{\psi}$ is linearly proportional to the tilt angle ϑ, since $\omega_3 \approx \dot{\psi}$ for small tilt angles (see (33)). That is, to steer the unicycle, it is necessary to tilt it accordingly.

Note that one may steer the unicycle with a specific yaw rate $\dot{\psi}_*$ in (42) even with zero tilt angle, but the model must be linearized around the nontilted turning steady state of the unicycle. This is left for future research.

B. Maneuvering

In this study, two maneuvers are considered for the steering control of the unicycle: a lane change and a 90° right turn, while assuming that the unicycle initially travels along the x_0-axis. Considering the steady-state velocity $v_{\mathrm{G}*} = R\dot{\varphi}_*$ of the center of gravity leads to the critical speed $v_{\mathrm{G,crit}} = (Rg/2)^{1/2}$ for the critical pitch rate $\dot{\varphi}_{\mathrm{crit}}$ in (51). For the parameters in Table I, we obtain $v_{\mathrm{G,crit}} \approx 1.21$ m/s. Thus, the lane change and right turn maneuvers are investigated for two speeds: $v_{\mathrm{G1}} = 1$ m/s which is below the critical speed, and $v_{\mathrm{G2}} = 5$ m/s which is above the critical speed.

When designing the controllers to execute these maneuvers, the nonreachable states ω_2, ω_3, φ, and x_{G} are omitted [see (35) and (54)]. Then, according to the state matrix (47) and the input matrix (52), the reduced system becomes

$$\begin{aligned}
\dot{\omega}_1 &= \left(\frac{4g}{5R} - \frac{12}{5}\dot{\varphi}_*^2\right)\vartheta - \frac{4m_0 g}{5mR^2}r + \frac{4}{5mR}u\,,\\
\dot{\vartheta} &= \omega_1\,,\\
\dot{\sigma} &= \left(2\dot{\varphi}_*^2 R - g\right)\vartheta + \frac{1}{m_0}u\,,\\
\dot{r} &= \sigma + R\omega_1\,,\\
\dot{\psi} &= -2\dot{\varphi}_*\vartheta\,,\\
\dot{y}_{\mathrm{G}} &= -R\omega_1 + \dot{\varphi}_* R\psi\,,
\end{aligned} \tag{57}$$

where the tildes above the states (representing perturbations) are omitted since the equilibrium values are zeros for all these states. We formally define the states in this reduced system as outputs of the full linear system $\dot{\tilde{\mathbf{x}}} = \mathrm{A}\tilde{\mathbf{x}} + \mathbf{B}u$ when designing the controllers for the lane change and turning maneuvers.

1) Lane Change: For the lane change maneuver, the state y_{G} can be utilized to plan the motion since the unicycle should move parallel to the x_0-axis at the beginning and at the end of the maneuver. According to this, we consider the output

$$\mathbf{y} = \mathbf{C}\mathbf{x} := \begin{bmatrix}\omega_1 & \vartheta & \sigma & r & \psi & y_{\mathrm{G}}\end{bmatrix}^{\top} \tag{58}$$

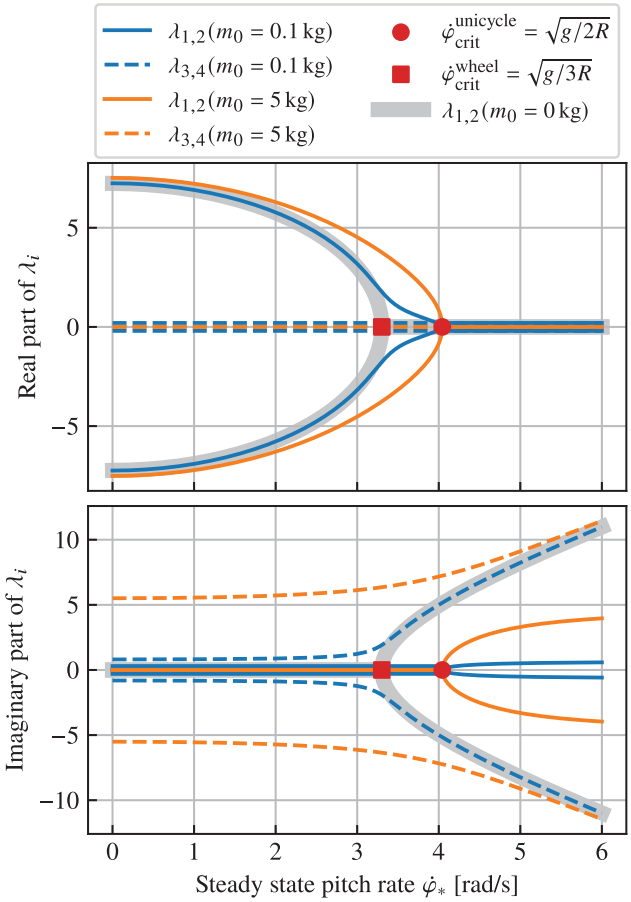

Fig. 7. Characteristic roots as a function of the steady-state pitch rate $\dot{\varphi}_*$ for straight rolling comparing the cases of rolling wheel and unicycle.

[see (57)] with

$$\mathbf{C} = \begin{bmatrix}
1 & 0 & 0 & 0 & 0 & 0 & 0 & 0 & 0 & 0\\
0 & 0 & 0 & 1 & 0 & 0 & 0 & 0 & 0 & 0\\
0 & 0 & 0 & 0 & 1 & 0 & 0 & 0 & 0 & 0\\
0 & 0 & 0 & 0 & 0 & 1 & 0 & 0 & 0 & 0\\
0 & 0 & 0 & 0 & 0 & 0 & 1 & 0 & 0 & 0\\
0 & 0 & 0 & 0 & 0 & 0 & 0 & 0 & 0 & 1
\end{bmatrix}. \tag{59}$$

The output controllability matrix can be constructed as

$$\mathbf{M}_{\mathrm{oc}} = \begin{bmatrix}\mathbf{CB} & \mathbf{CAB} & \mathbf{CA}^2\mathbf{B} & \dots & \mathbf{CA}^9\mathbf{B}\end{bmatrix} \tag{60}$$

which has a maximal row rank, $\operatorname{rank}\mathbf{M}_{\mathrm{oc}} = 6$. That is, the unicycle is output controllable.

Then, we apply the linear output feedback law

$$u := -\mathbf{K}\left(\mathbf{y} - \mathbf{y}_{\mathrm{des}}\right) \tag{61}$$

with control gains $\mathbf{K} = [D_\vartheta\ P_\vartheta\ D_r\ P_r\ P_\psi\ P_y]$ and

$$\mathbf{y}_{\mathrm{des}} = \begin{bmatrix}0 & 0 & 0 & 0 & 0 & y_{\mathrm{des}}(t)\end{bmatrix}^{\top}, \tag{62}$$

where $y_{\mathrm{des}}(t)$ encodes the desired trajectory in terms of y_{G}.

Here, we consider

$$y_{\mathrm{des}}(t) = \begin{cases}
0, & 0 \le t < 2\,,\\
\dfrac{L}{2}\left(\cos\left(\frac{\pi}{5}(t-2)\right) - 1\right), & 2 \le t < 7\,,\\
-L, & 7 \le t < 10\,,
\end{cases} \tag{63}$$

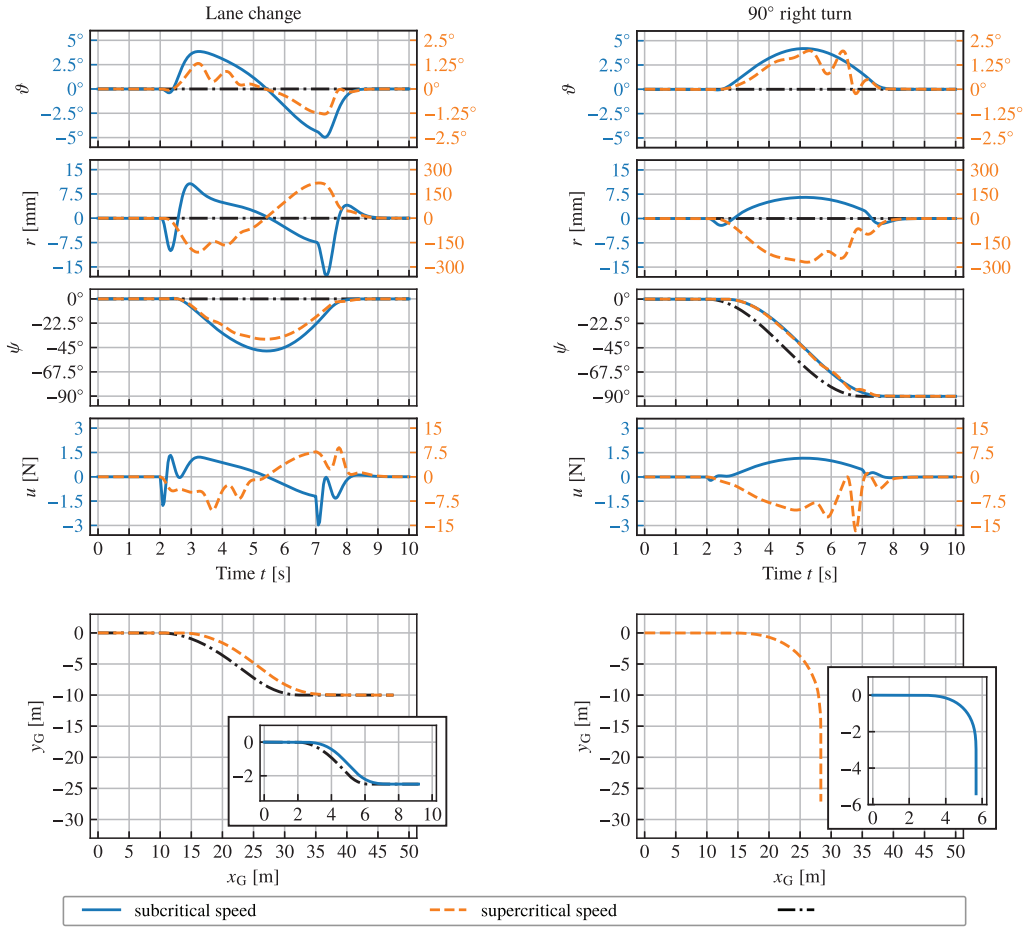

Fig. 8. Maneuvers: lane change (left column) and 90° right turn (right column) below the critical speed (solid blue) and above (dashed orange).

and we use $L = 2.5\,\mathrm{m}$ for speed $v_{\mathrm{G1}} = 1$ m/s and $L = 10\,\mathrm{m}$ for speed $v_{\mathrm{G2}} = 2$ m/s. The desired trajectories are depicted as black dashed–dotted curves in the (x_0, y_0)-plane in the bottom left panel in Fig. 8. For simplicity, we consider the desired yaw angle $\psi_{\mathrm{des}}(t) \equiv 0$ in (62). More sophisticated reference trajectories might be constructed utilizing (38).

Note that the proposed linear controller does not ensure the global stability of the nonlinear system. Nonlinear investigations are outside the scope of the present study. Also, maneuvers with substantial nonzero $\dot{\psi}$ may make the unicycle deviate significantly from the straight rolling steady state, which may cause a large deviation in the observed behavior.

The characteristic equation of the closed-loop system is

$$\det\left(\lambda \mathbf{I} - (\mathbf{A} - \mathbf{BKC})\right) = 0\,. \tag{64}$$

By selecting the control gains in $\mathbf{K}$ in (61) appropriately, one may place the nonzero characteristic roots to the left half complex plane and guarantee stability for the closed-loop system. In particular, using the control gains in Table II results in $\lambda_{\mathrm{k}} = -8\mathrm{s}^{-1}$, $k = 1, \ldots, 6$.

The performance of the closed-loop system is demonstrated by numerical simulations in the left column in Fig. 8. These were carried out using the full nonlinear equations (34) applying the control law (61) with reference trajectory (63) and control gains in Table II. The time evolution of the tilt angle ϑ, point mass position r, yaw angle ψ, and the control input u are depicted in the top four panels, while the bottom panel shows the movement of the wheel center G above the (x_0, y_0)-plane. The desired lane change maneuver is followed by the unicycle, and the controller successfully stabilizes the desired motion for both speeds. The gains P_ϑ and D_ϑ are highlighted in Table II as they have opposite signs above and below the critical speed. Below the critical speed ($v_{\mathrm{G1}} < v_{\mathrm{G,crit}}$), the open-loop dynamics is unstable; here, the P_ϑ and D_ϑ gains correspond to positive stiffness and damping in the mechanical sense, respectively. In contrast, above the critical speed ($v_{\mathrm{G2}} > v_{\mathrm{G,crit}}$), the open-loop dynamics is stable and the P_ϑ and D_ϑ gains correspond to negative stiffness and damping. This illustrates that executing a lane change maneuver above the critical speed takes more effort, since the straight-rolling motion of the open-loop systems is more stable. This can also be observed when comparing the required control input for the different speeds. Still, the required control input remains small ($|u| < 10\mathrm{N}$) for both speeds.

2) Right Turn: For the 90° right turn maneuver, the unicycle eventually moves parallel to the y_0-axis and the state y_{G} becomes unreachable by the control input. Thus, the state y_{G} may not be used to plan motion in this case. Instead, we use the

TABLE II
CONTROL GAINS FOR THE LANE CHANGE MANEUVER

Below critical speed $v_{G1} < v_{G,crit}$		Above critical speed $v_{G2} > v_{G,crit}$	
D_ϑ	**−1407.64**Ns	D_ϑ	**105.36**Ns
P_ϑ	**−7637.29**N	P_ϑ	**777.28**N
D_r	2116.86Ns/m	D_r	99.52Ns/m
P_r	11942.04N/m	P_r	405.60N/m
P_ψ	3382.02N	P_ψ	676.4N
P_y	4509.36N/m	P_y	180.37N/m

TABLE III
CONTROL GAINS FOR THE TURNING MANEUVER

Below critical speed $v_{G1} < v_{G,crit}$		Above critical speed $v_{G2} > v_{G,crit}$	
D_ϑ	**−511.89**Ns	D_ϑ	**118.88**Ns
P_ϑ	−2776.88N	P_ϑ	−128.32N
D_r	882.53Ns/m	D_r	41.49Ns/m
P_r	4881.84N/m	P_r	73.69N/m
P_ψ	536.67N	P_ψ	112.73N

yaw angle ψ to construct the reference trajectory. Considering this, the output vector

$$\mathbf{y} = \mathbf{C}\mathbf{x} := \begin{bmatrix} \omega_1 & \vartheta & \sigma & r & \psi \end{bmatrix}^\top \tag{65}$$

with

$$\mathbf{C} = \begin{bmatrix} 1 & 0 & 0 & 0 & 0 & 0 & 0 & 0 & 0 & 0 \\ 0 & 0 & 0 & 1 & 0 & 0 & 0 & 0 & 0 & 0 \\ 0 & 0 & 0 & 0 & 1 & 0 & 0 & 0 & 0 & 0 \\ 0 & 0 & 0 & 0 & 0 & 1 & 0 & 0 & 0 & 0 \\ 0 & 0 & 0 & 0 & 0 & 0 & 1 & 0 & 0 & 0 \end{bmatrix} \tag{66}$$

is defined [see (58) and (59)]. The output controllability matrix can be constructed as in (60); since it has maximal row rank, $\operatorname{rank} \mathbf{M}_{oc} = 5$, the unicycle is output controllable.

Here, the linear output feedback control law of the form (61) is applied with control gains $\mathbf{K} = [D_\vartheta \; P_\vartheta \; D_r \; P_r \; P_\psi]$ and

$$\mathbf{y}_{des} = \begin{bmatrix} 0 & 0 & 0 & 0 & \psi_{des}(t) \end{bmatrix}^\top \tag{67}$$

where the yaw angle

$$\psi_{des}(t) = \begin{cases} 0, & 0 \le t < 2, \\ \frac{\pi}{4}\left(1 - \cos\left(\frac{\pi}{5}(t-2)\right)\right), & 2 \le t < 7, \\ \frac{\pi}{2}, & 7 \le t < 10, \end{cases} \tag{68}$$

encodes the desired trajectory. Such a trajectory is depicted as a black dashed–dotted curve in Fig. 8 (right column, third panel). Choosing the control gains as in Table III for the speeds v_{G1} and v_{G2} the nonzero characteristic roots of the closed-loop system are placed at $\lambda_k = -8\text{s}^{-1}$, $k = 1, \ldots, 5$. Since these are in the left half complex plane, the resulting closed-loop system is stable.

The simulation results are shown on the right side of Fig. 8. These are carried out using the full nonlinear equations (34) applying the feedback law (61) with reference trajectory (67) and control gains in Table III. The right turns are successfully executed for both speeds. Comparing the control gains below and above the critical speed for the turning maneuver, only the derivative gain D_ϑ changes sign as highlighted in Table III. When observing the time evolution of the states and the control input in Fig. 8, one may notice some high-frequency content which is more pronounced above the critical speed (orange curves). These are due to the Coriolis force since the yaw rate is not zero while the point mass moves along the axle. These effects are compensated by the controller while executing the maneuvers.

V. CONCLUSION

In this study, the modeling, analysis, and control of an autonomous unicycle were considered. The most compact form of the equations of motion was derived using the Appellian approach. The steady-state motions of the rolling wheel were classified as cases of straight rolling, turning-rolling, and spinning on the spot. The stability of these motions was determined by linear analysis, and the critical angular velocities (above which the steady-state motions are stable) were given in closed form. It was also shown that a turning-rolling steady state is always stable above a critical tilt angle, which is independent of the system parameters.

Building upon the knowledge gained from the dynamics of the rolling wheel, the simplest possible control strategy is proposed for autonomous unicycles by means of actuating the position of a point mass normal to the wheel plane, to accomplish steering maneuvers such as lane changes and turns. The nonlinear equations of motion of the unicycle were given in closed form. Apart from finding steady states akin to those of the rolling wheel, additional steady states were identified, such as nontilted turning and tilted spinning. For the open-loop unicycle, stability results were obtained for the straight rolling steady state, and the stability of the turning-rolling steady states was determined semi-analytically, numerically. All these stability results rely on linearization; the analysis of the conserved quantities is reserved for future research.

Utilizing the equations linearized about the straight rolling steady state, two steering controllers of partial state feedback were proposed for the unicycle to carry out a lane change and a 90° turn. The resulting linear systems were shown to be output controllable, and when applying the designed controllers to the nonlinear system, the unicycle successfully completed the desired maneuvers as confirmed by numerical simulations.

The developed modeling, analysis, and control framework may also allow more sophisticated motion planning as well as nonlinear control design, which can take full advantage of the agility of unicycles. Such techniques, which are left for future research, may allow one to achieve a high level of maneuverability for autonomous unicycles and to provide steering assistance for human-ridden unicycles.

The introduced unicycle model incorporates engineering assumptions, which do not necessarily hold in all circumstances. For example, sliding may occur, violating the rolling assumption once the friction forces are not large enough. This will be analyzed in a separate study. Also, experiments are

planned with the human-ridden and the autonomous unicycles to verify the theoretical findings.

APPENDIX A
MODEL DERIVATION FOR THE ROLLING WHEEL VIA THE APPELLIAN APPROACH

A vector resolved in frame F_2 can be transformed to the frame F_0 as

$$\square_{\mathrm{F}_0} = \mathbf{T}_{02}\square_{\mathrm{F}_2} \tag{69}$$

where the rotation matrix is

$$\mathbf{T}_{02} = \begin{bmatrix} \cos\psi & -\sin\psi\cos\vartheta & \sin\psi\sin\vartheta \\ \sin\psi & \cos\psi\cos\vartheta & -\cos\psi\sin\vartheta \\ 0 & \sin\vartheta & \cos\vartheta \end{bmatrix}. \tag{70}$$

The velocity of the wheel–ground contact point P can be expressed as

$$\mathbf{v}_{\mathrm{P}} = \mathbf{v}_{\mathrm{G}} + \boldsymbol{\omega} \times \mathbf{r}_{\mathrm{GP}} \tag{71}$$

where the velocity of the center of gravity G can be resolved in the ground-fixed frame F_0 as

$$\mathbf{v}_{\mathrm{G}} = \dot{\mathbf{r}}_{\mathrm{G}} = \begin{bmatrix} \dot{x}_{\mathrm{G}} & \dot{y}_{\mathrm{G}} & \dot{z}_{\mathrm{G}} \end{bmatrix}^{\top}_{\mathrm{F}_0} \tag{72}$$

while the angular velocity of the wheel can be expressed in the moving frame F_2 as

$$\boldsymbol{\omega} = \begin{bmatrix} \dot{\vartheta} & \dot{\psi}\sin\vartheta + \dot{\varphi} & \dot{\psi}\cos\vartheta \end{bmatrix}^{\top}_{\mathrm{F}_2} \tag{73}$$

using the tilt rate $\dot{\vartheta}$, the yaw rate $\dot{\psi}$, the pitch rate $\dot{\varphi}$, and the tilt angle ϑ. One may also express the position vector as

$$\mathbf{r}_{\mathrm{GP}} = \begin{bmatrix} 0 & 0 & -R \end{bmatrix}^{\top}_{\mathrm{F}_2}. \tag{74}$$

Then, transforming the cross product in (71) to the ground-fixed frame F_0 with the help of (70), the rolling condition (1) results in the kinematic constraints (2) and the geometric constraint (3).

The definitions of pseudovelocities are appropriate only if the generalized velocities $(\dot{x}_{\mathrm{G}}, \dot{y}_{\mathrm{G}}, \dot{\psi}, \dot{\vartheta}, \dot{\varphi})$ can unambiguously be expressed using the pseudovelocities $(\omega_1, \omega_2, \omega_3)$ and generalized coordinates $(x_{\mathrm{G}}, y_{\mathrm{G}}, \psi, \vartheta, \varphi)$. To check this, we combine the kinematic constraints (2) and the definitions of pseudovelocities (5) into one linear system of equations as (75), shown at the bottom of the page.

This linear system can be solved if $\mathbf{C}$ is invertible, that is, if its determinant is nonzero. Since $\det\mathbf{C} = \cos\vartheta$, the matrix $\mathbf{C}$ is singular when the wheel is horizontal ($\vartheta = \pm\pi/2$), which is excluded from this analysis. Thus, the generalized velocities $(\dot{x}_{\mathrm{G}}, \dot{y}_{\mathrm{G}}, \dot{\psi}, \dot{\vartheta}, \dot{\varphi})$ can be expressed with the pseudovelocities $(\omega_1, \omega_2, \omega_3)$ as

$$\begin{aligned} \dot{x}_{\mathrm{G}} &= \omega_1 R\sin\psi\cos\vartheta + \omega_2 R\cos\psi, \\ \dot{y}_{\mathrm{G}} &= -\omega_1 R\cos\psi\cos\vartheta + \omega_2 R\sin\psi, \\ \dot{\psi} &= \omega_3\frac{1}{\cos\vartheta}, \quad \dot{\vartheta} = \omega_1, \quad \dot{\varphi} = \omega_2 - \omega_3\tan\vartheta. \end{aligned} \tag{76}$$

Also, the velocity of the center of gravity G (72) and the angular velocity (73) can be expressed in the terms of pseudovelocities $(\omega_1, \omega_2, \omega_3)$ using (76); these vectors have the most compact form when expressed in frame F_2

$$\begin{aligned} \mathbf{v}_{\mathrm{G}} &= \begin{bmatrix} \dot{\psi}R\sin\vartheta + \dot{\varphi}R & -\dot{\vartheta}R & 0 \end{bmatrix}^{\top}_{\mathrm{F}_2} \equiv \begin{bmatrix} \omega_2 R & -\omega_1 R & 0 \end{bmatrix}^{\top}_{\mathrm{F}_2}, \\ \boldsymbol{\omega} &= \begin{bmatrix} \dot{\vartheta} & \dot{\psi}\sin\vartheta + \dot{\varphi} & \dot{\psi}\cos\vartheta \end{bmatrix}^{\top}_{\mathrm{F}_2} \equiv \begin{bmatrix} \omega_1 & \omega_2 & \omega_3 \end{bmatrix}^{\top}_{\mathrm{F}_2}. \end{aligned} \tag{77}$$

The acceleration energy of a rigid body is defined as

$$S = \frac{1}{2}m\mathbf{a}_{\mathrm{G}}^2 + \frac{1}{2}\boldsymbol{\alpha}\cdot\mathbf{J}_{\mathrm{G}}\boldsymbol{\alpha} + \boldsymbol{\alpha}\cdot(\boldsymbol{\omega}\times\mathbf{J}_{\mathrm{G}}\boldsymbol{\omega}) \tag{78}$$

where $\mathbf{a}_{\mathrm{G}} = \dot{\mathbf{v}}_{\mathrm{G}}$ is the acceleration of the center of gravity, $\boldsymbol{\alpha} = \dot{\boldsymbol{\omega}}$ is the angular acceleration, and $\mathbf{J}_{\mathrm{G}}$ is the mass moment of inertia with respect to the center of gravity. All these vectors must be expressed based on the generalized coordinates $(x_{\mathrm{G}}, y_{\mathrm{G}}, \psi, \vartheta, \varphi)$, pseudovelocities $(\omega_1, \omega_2, \omega_3)$, and pseudoaccelerations $(\dot{\omega}_1, \dot{\omega}_2, \dot{\omega}_3)$. Also, the vectors have the most compact form when expressed in the frame F_2

$$\begin{aligned} \mathbf{a}_{\mathrm{G}} &= \begin{bmatrix} R(\dot{\omega}_2 + \omega_1\omega_3) \\ -R(\dot{\omega}_1 - \omega_2\omega_3) \\ -R\left(\omega_1^2 + \omega_2\omega_3\tan\vartheta\right) \end{bmatrix}_{\mathrm{F}_2}, \quad \mathbf{J}_{\mathrm{G}} = \frac{mR^2}{4}\begin{bmatrix} 1 & 0 & 0 \\ 0 & 2 & 0 \\ 0 & 0 & 1 \end{bmatrix}_{\mathrm{F}_2}, \\ \boldsymbol{\alpha} &= \begin{bmatrix} \dot{\omega}_1 - \omega_2\omega_3 + \omega_3^2\tan\vartheta \\ \dot{\omega}_2 \\ \dot{\omega}_3 + \omega_1\omega_2 - \omega_1\omega_3\tan\vartheta \end{bmatrix}_{\mathrm{F}_2}. \end{aligned} \tag{79}$$

The calculation of the accelerations is not trivial in the moving frame F_2; still, this gives the simplest possible algebraic form.

These lead to the acceleration energy of the rolling disk

$$\begin{aligned} S = \frac{mR^2}{8}\Big(&5\dot{\omega}_1^2 + 6\dot{\omega}_2^2 + \dot{\omega}_3^2 + \left(2\omega_3^2\tan\vartheta - 12\omega_2\omega_3\right)\dot{\omega}_1 \\ &+8\omega_1\omega_3\dot{\omega}_2 + \left(4\omega_1\omega_2 - 2\omega_1\omega_3\tan\vartheta\right)\dot{\omega}_3\Big) + \cdots, \end{aligned} \tag{80}$$

where the dots $(\ldots)$ represent further terms that are independent of the pseudoaccelerations $(\dot{\omega}_1, \dot{\omega}_2, \dot{\omega}_3)$, so they can be neglected.

Appell's equations are formulated as

$$\frac{\partial S}{\partial\dot{\sigma}_j} = \Pi_j, \quad j = 1, \ldots, 3 \tag{81}$$

$$\begin{bmatrix} 0 \\ 0 \\ \omega_1 \\ \omega_2 \\ \omega_3 \end{bmatrix} = \underbrace{\begin{bmatrix} -1 & 0 & R\sin\vartheta\cos\psi & R\sin\psi\cos\vartheta & R\cos\psi \\ 0 & -1 & R\sin\psi\sin\vartheta & -R\cos\psi\cos\vartheta & R\sin\psi \\ 0 & 0 & 0 & 1 & 0 \\ 0 & 0 & \sin\vartheta & 0 & 1 \\ 0 & 0 & \cos\vartheta & 0 & 0 \end{bmatrix}}_{\mathbf{C}} \begin{bmatrix} \dot{x}_{\mathrm{G}} \\ \dot{y}_{\mathrm{G}} \\ \dot{\psi} \\ \dot{\vartheta} \\ \dot{\varphi} \end{bmatrix}. \tag{75}$$

where Π_j is the pseudoforce corresponding to the pseudoacceleration $\dot{\omega}_j$. The pseudoforces can be calculated from the virtual power of the active forces

$$\delta P = \mathbf{G} \cdot \delta \mathbf{v}_\mathrm{G} = \sum_{j=1}^{3} \Pi_j \, \delta\omega_j \,. \tag{82}$$

Here, $\mathrm{G} = [0 \;\; 0 \;\; -mg]^\top_{\mathrm{F}_0}$ represents the gravitational force, the only active force in our model, while $\delta\mathbf{v}_\mathrm{G} = [\delta\dot{x}_\mathrm{G} \;\; \delta\dot{y}_\mathrm{G} \;\; \delta\dot{z}_\mathrm{G}]^\top_{\mathrm{F}_0} = [\cdot \;\; \cdot \;\; -R\sin\vartheta\,\delta\omega_1]^\top_{\mathrm{F}_0}$ represents the virtual velocity [see (72)]. These yield the pseudoforces

$$\Pi_1 = mgR\sin\vartheta \,, \quad \Pi_2 = 0 \,, \quad \Pi_3 = 0 \,. \tag{83}$$

Based on the acceleration energy (80), Appell's formula (81), and the pseudoforces (83), the pseudoaccelerations can be expressed as

$$\begin{aligned} \dot{\omega}_1 &= \frac{6}{5}\omega_2\omega_3 - \frac{1}{5}\omega_3^2\tan\vartheta + \frac{4g}{5R}\sin\vartheta \,, \\ \dot{\omega}_2 &= -\frac{2}{3}\omega_1\omega_3 \,, \\ \dot{\omega}_3 &= -2\omega_1\omega_2 + \omega_1\omega_3\tan\vartheta. \end{aligned} \tag{84}$$

These equations, together with the generalized velocities (76), form the system of eight first-order ordinary differential equations, which constitute the equations of the motion of the rolling wheel [see (6)].

Appendix B
Stability of the Rolling Wheel

To prove the stability of the steady states of the rolling wheel, we follow [31]. First, time is eliminated from the second and third equations of the essential motion (6) by expressing

$$\omega_2' = -2\omega_3/3 \,, \quad \omega_3' = -2\omega_2 + \omega_3\tan\vartheta \tag{85}$$

where $\omega_2' = (d\omega_2/d\vartheta)$, $\omega_3' = (d\omega_3/d\vartheta)$ and $\dot{\vartheta} = \omega_1$. Since the wheel is a conservative mechanical system, the total energy $E = T+U$ is constant, $E(t) \equiv E_*$, where $T = mR^2(5\omega_1^2+6\omega_2^2+\omega_3^2)/8$ and $U = mgR\cos\vartheta$ are the kinetic and potential energies of the wheel, respectively. Rearranging the total energy gives

$$\omega_1^2 \equiv \dot{\vartheta}^2 = \underbrace{\frac{1}{5mR^2}\left(8E_* - mR\left(6\omega_2^2R - \omega_3^2R - 8g\cos\vartheta\right)\right)}_{= f\left(\vartheta;\, \vartheta_\mathrm{ic}, \omega_{2,\mathrm{ic}}, \omega_{3,\mathrm{ic}}, E_*\right)} . \tag{86}$$

The condition for stability is that f has a strict maximum at $\vartheta = \vartheta_*$. Expressing $df/d\vartheta = 0$ gives back formula (12) representing the steady-state surface in Fig. 3. The necessary and sufficient condition for steady states to be stable can be obtained with $d^2f/d\vartheta^2 < 0$, where (85) is substituted. This leads to (20) which is obtained from analyzing the linearized systems.

Appendix C
Model Derivation for the Unicycle via the Appellian Approach

With the added point mass the definition (33) of pseudovelocities is appropriate because the generalized velocities ($\dot{x}_\mathrm{G}$, $\dot{y}_\mathrm{G}$, $\dot{\psi}$, $\dot{\vartheta}$, $\dot{\varphi}$, $\dot{r}$) can unambiguously be expressed by means of the pseudovelocities (ω_1, ω_2, ω_3, σ) and the generalized coordinates (x_G, y_G, ψ, ϑ, φ, r) when (76) is extended with $\dot{r} = \sigma + \omega_1 R$.

The acceleration energy S of the unicycle consisting of the rigid wheel and the point mass is defined as

$$S = \frac{1}{2}m\mathbf{a}_\mathrm{G}^2 + \frac{1}{2}\boldsymbol{\alpha}\cdot\mathbf{J}_\mathrm{G}\boldsymbol{\alpha} + \boldsymbol{\alpha}\cdot(\boldsymbol{\omega}\times\mathbf{J}_\mathrm{G}\boldsymbol{\omega}) + \frac{1}{2}m_0\mathbf{a}_\mathrm{A}^2 \tag{87}$$

where the first three terms are identical to those in (78) and (79). The velocity $\mathbf{v}_\mathrm{A}$ of the point mass m_0 can be expressed as

$$\mathbf{v}_\mathrm{A} = \begin{bmatrix} \dot{\psi}\,(R\sin\vartheta - r\cos\vartheta) + \dot{\varphi}R \\ \dot{r} - \dot{\vartheta}R \\ \dot{\vartheta}r \end{bmatrix}_{\mathrm{F}_2} \equiv \begin{bmatrix} \omega_2 R - \omega_3 r \\ \sigma \\ \omega_1 r \end{bmatrix}_{\mathrm{F}_2} \tag{88}$$

while the acceleration $\mathbf{a}_\mathrm{A}$ becomes

$$\mathbf{a}_\mathrm{A} = \begin{bmatrix} \dot{\omega}_2 R - \dot{\omega}_3 r + \omega_1\omega_3\,(r\tan\vartheta - R) - 2\omega_3\sigma \\ \dot{\sigma} - \omega_1^2 r - \omega_3^2 r + \omega_2\omega_3 R \\ \dot{\omega}_1 r + \omega_1^2 R + 2\omega_1\sigma + \omega_3^2 r\tan\vartheta - \omega_2\omega_3 R\tan\vartheta \end{bmatrix}_{\mathrm{F}_2} . \tag{89}$$

These lead to

$$\begin{aligned} S = {} & \frac{1}{8}\left(5mR^2 + 4m_0r^2\right)\dot{\omega}_1^2 + \frac{1}{4}\left(3m + 2m_0\right)R^2\dot{\omega}_2^2 \\ & + \frac{1}{8}\left(mR^2 + 4m_0r^2\right)\dot{\omega}_3^2 + \frac{m_0}{2}\dot{\sigma}^2 - m_0Rr\dot{\omega}_2\dot{\omega}_3 \\ & + \frac{1}{4}\left(4\omega_1^2 m_0 Rr + 8\omega_1\sigma m_0 r + \omega_3^2\left(mR^2 + 4m_0r^2\right)\tan\vartheta \right. \\ & \qquad \left. -\omega_2\omega_3\left(6mR^2 + 4m_0Rr\tan\vartheta\right)\right)\dot{\omega}_1 \\ & + \left(\omega_1\omega_3\left(mR^2 - m_0R^2 + m_0Rr\tan\vartheta\right) - 2\omega_3\omega m_0R\right)\dot{\omega}_2 \\ & + \frac{1}{4}\left(2\omega_1\omega_2 mR^2 + \omega_1\omega_3\left(4m_0Rr - mR^2\tan\vartheta \right.\right. \\ & \qquad \left.\left. -4m_0r^2\tan\vartheta\right) + 8\omega_3\sigma m_0 r\right)\dot{\omega}_3 \\ & + \left(\omega_2\omega_3 m_0 R - \omega_1^2 m_0 r - \omega_3^2 m_0 r\right)\dot{\sigma} + \ldots \,. \end{aligned} \tag{90}$$

The pseudoforces Π_j are expressed based on the virtual power

$$\delta P = \mathbf{G}\cdot\delta\mathbf{v}_\mathrm{G} + \mathbf{G}_\mathrm{A}\cdot\delta\mathbf{v}_\mathrm{A} + \mathbf{F}\cdot\delta\mathbf{v}_\mathrm{A} - \mathbf{F}\cdot\delta\mathbf{v}_\mathrm{G} = \sum_{j=1}^{4}\Pi_j\,\delta\omega_j \tag{91}$$

where $\mathrm{G} = [0 \;\; 0 \;\; -mg]^\top_{\mathrm{F}_0}$ and $\mathrm{G}_\mathrm{A} = [0 \;\; 0 \;\; -m_0g]^\top_{\mathrm{F}_0}$ are the gravitational forces acting on the wheel and the point mass, respectively, $\delta\mathbf{v}_\mathrm{A} = [R\delta\omega_2 - r\delta\omega_3 \;\; \delta\sigma \;\; r\delta\omega_1]^\top_{\mathrm{F}_2}$, $\mathbf{F}$ is the control force (31) and we used the notation $\omega_4 = \sigma$. This yields the following pseudoforces:

$$\begin{aligned} \Pi_1 &= (m + m_0)\,gR\sin\vartheta - m_0gr\cos\vartheta \,, \\ \Pi_2 &= 0 \,, \quad \Pi_3 = 0 \,, \quad \Pi_4 = u - m_0g\sin\vartheta \,. \end{aligned} \tag{92}$$

In the case of $m_0 > 0$, the pseudoaccelerations ($\dot{\omega}_1$, $\dot{\omega}_2$, $\dot{\omega}_3$, $\dot{\sigma}$) can be obtained from the Appellian equations of the form (81), while the generalized velocities ($\dot{x}_\mathrm{G}$, $\dot{y}_\mathrm{G}$, $\dot{\psi}$, $\dot{\vartheta}$, $\dot{\varphi}$, $\dot{r}$) can

also be expressed from the definition of the pseudovelocities (33) and the kinematic constraints (2) for $\vartheta \neq \pm\pi/2$. These result in the equations of motion of the unicycle (34).

APPENDIX D
ELEMENTS OF MATRIX A IN (45)

Note that in the following formulas, the steady-state tilt angle ϑ_*, yaw rate $\dot{\psi}_*$, pitch rate $\dot{\varphi}_*$, and point mass position r_* are not independent of each other but they must satisfy the relations in (38)

$$A_{12} = \frac{\dot{\psi}_* \left(6mR^2 \cos\vartheta_* + 4m_0 R r_* \sin\vartheta_*\right)}{5mR^2 + 4m_0 r_*^2},$$

$$A_{13} = \frac{1}{5mR^2 + 4m_0 r_*^2} \left(\dot{\varphi}_* R \left(6mR + 4m_0 r_* \tan\vartheta_*\right) + \dot{\psi}_* \left(4m_0 R r_* \tan\vartheta_* + \left(4mR^2 - 8\ m_0 r_*^2\right)\right) \sin\vartheta_*\right),$$

$$A_{14} = \frac{1}{\left(5mR^2 + 4m_0 r_*^2\right)\cos\vartheta_*} \cdot \left(4\dot{\psi}_* \dot{\varphi}_* m_0 R r_* + \dot{\psi}_*^2 \left(4m_0 R r_* \tan\vartheta_* - \left(mR^2 + 4m_0 r_*^2\right)\right)\cos\vartheta_* + 4m_0 g r_* \sin\vartheta_* \cos\vartheta_* + 4mgR\cos^2\vartheta_*\right),$$

$$A_{16} = \frac{m_0}{\left(5mR^2 + 4m_0 r_*^2\right)^2} \cdot \left(\left(16m_0 g r_*^2 - 20\ mgR^2\right)\cos\vartheta_* + \dot{\psi}_* \dot{\varphi}_* \cdot \left(\left(20mR^3 - 16\ m_0 R r_*^2\right)\sin\vartheta_* - 48\ mR^2 r_* \cos\vartheta_*\right) - 32\ mgR r_* \sin\vartheta_* + 4\dot{\psi}_*^2 \left(\left(5mR^3 - 4m_0 R r_*^2\right)\sin^2\vartheta_* - 20\ mR^2 r_* \sin\vartheta_* \cos\vartheta_*\right)\right),$$

$$A_{21} = \frac{1}{3mR^2 + 2\ m_0 R^2 + 12\ m_0 r_*^2} \cdot \left(-4R\dot{\varphi}_* m_0 r_* + 2\dot{\psi}_* \left(\left(m_0 R^2 - mR^2 - 4m_0 r_*^2\right) \cdot \cos\vartheta_* - 2\ m_0 R r_* \sin\vartheta_*\right)\right),$$

$$A_{25} = \frac{4R\dot{\psi}_* m_0 \cos\vartheta_*}{3mR^2 + 2\ m_0 R^2 + 12\ m_0 r_*^2},$$

$$A_{31} = \frac{1}{3mR^2 + 2\ m_0 R^2 + 12\ m_0 r_*^2} \cdot \left(-\dot{\varphi}_* \left(6\ mR^2 + 4m_0 R^2\right) + \dot{\psi}_* \left(\left(12m_0 r_*^2 - 3mR^2 - 2\ m_0 R^2\right)\sin\vartheta_* - 20\ m_0 R r_* \cos\vartheta_*\right)\right),$$

$$A_{35} = -\frac{24\dot{\psi}_* m_0 r_* \cos\vartheta_*}{3mR^2 + 2\ m_0 R^2 + 12\ m_0 r_*^2},$$

$$A_{52} = -\dot{\psi}_* R\cos\vartheta_*,\quad A_{53} = \dot{\psi}_* \left(2\ r_* \cos\vartheta_* - R\sin\vartheta_*\right) - \dot{\varphi}_* R,$$

$$A_{54} = -g\cos\vartheta_*,\quad A_{56} = \dot{\psi}_*^2 \cos^2\vartheta_*,\quad A_{61} = R,$$

$$A_{73} = \frac{1}{\cos\vartheta_*},\quad A_{74} = \dot{\psi}_* \tan\vartheta_*,\quad A_{83} = -\tan\vartheta_*,$$

$$A_{84} = -\frac{\dot{\psi}_*}{\cos\vartheta_*},\quad A_{91} = R\sin\psi_* \cos\vartheta_*,\quad A_{92} = R\cos\psi_*,$$

$$A_{97} = -R\left(\dot{\psi}_* \sin\vartheta_* + \dot{\varphi}_*\right)\sin\psi_*,\quad A_{101} = -R\cos\psi_* \cos\vartheta_*,$$

$$A_{102} = R\sin\psi_*,\quad A_{107} = R\left(\dot{\psi}_* \sin\vartheta_* + \dot{\varphi}_*\right)\cos\psi_*.$$

REFERENCES

[1] M. Dozza, T. Li, L. Billstein, C. Svernlöv, and A. Rasch, "How do different micro-mobility vehicles affect longitudinal control? Results from a field experiment," *J. Saf. Res.*, vol. 84, pp. 24–32, Feb. 2023.

[2] C. Ozaka, H. Kano, and M. Masubuchi, "Stability of a monocycle-type inverted pendulum," in *Proc. 3rd Vehicle Autom. Symp. Jpn. Autom. Control Soc.*, 1980, pp. 63–66.

[3] A. Schoonwinkel, "Design and test of a computer stabilized unicycle," Ph.D. thesis, Dept. Aeronaut. Astronaut., Stanford Univ., Stanford, CA, USA, 1987.

[4] D. W. Vos and A. H. Von Flotow, "Dynamics and nonlinear adaptive control of an autonomous unicycle: Theory and experiment," in *Proc. 29th IEEE Conf. Decis. Control*, vol. 1, Dec. 1990, pp. 182–187.

[5] Y. Naveh, P. Z. Bar-Yoseph, and Y. Halevi, "Nonlinear modeling and control of a unicycle," *Dyn. Control*, vol. 9, pp. 279–296, Oct. 1999.

[6] D. V. Zenkov, A. M. Bloch, and J. E. Marsden, "The Lyapunov–Malkin theorem and stabilization of the unicycle with rider," *Syst. Control Lett.*, vol. 45, no. 4, pp. 293–302, Apr. 2002.

[7] Y. Isomi and S. Majima, "Tracking control method for an underactuated unicycle robot using an equilibrium state," in *Proc. IEEE Int. Conf. Control Autom.*, Dec. 2009, pp. 1844–1849.

[8] X. Ruan, J. Hu, and Q. Wang, "Modeling with Euler–Lagrang equation and cybernetical analysis for a unicycle robot," in *Proc. 2nd Int. Conf. Intell. Comput. Technol. Autom.*, vol. 2, Oct. 2009, pp. 108–111.

[9] S. I. Han and J. M. Lee, "Balancing and velocity control of a unicycle robot based on the dynamic model," *IEEE Trans. Ind. Electron.*, vol. 62, no. 1, pp. 405–413, Jan. 2015.

[10] L. Zhao, X. Zhang, Q. Xu, and J. Ji, "Dynamics modeling and postural stability control of a unicycle robot," in *Proc. Int. Conf. Fluid Power Mechatronics (FPM)*, Aug. 2015, pp. 1123–1127.

[11] X. Cao, D. C. Bui, D. Takács, and G. Orosz, "Autonomous unicycle: Modeling, dynamics, and control," *Multibody Syst. Dyn.*, vol. 61, no. 1, pp. 43–76, May 2024.

[12] H. B. Brown and Y. Xu, "A single-wheel, gyroscopically stabilized robot," in *Proc. IEEE Int. Conf. Robot. Autom.*, vol. 4, Apr. 1996, pp. 3658–3663.

[13] M.-Q. Dao and K.-Z. Liu, "Gain-scheduled stabilization control of a unicycle robot," *JSME Int. J. Ser. C*, vol. 48, no. 4, pp. 649–656, 2005.

[14] K. G. Toiserkan and J. Kövecses, "Improving stability and performance of digitally controlled systems: The concept of modified holds," in *Proc. IEEE Int. Conf. Robot. Autom.*, May 2010, pp. 5173–5180.

[15] H. Jin, T. Wang, F. Yu, Y. Zhu, J. Zhao, and J. Lee, "Unicycle robot stabilized by the effect of gyroscopic precession and its control realization based on centrifugal force compensation," *IEEE/ASME Trans. Mechatronics*, vol. 21, no. 6, pp. 2737–2745, Dec. 2016.

[16] Z. Sheng and K. Yamafuji, "Study on the stability and motion control of a unicycle: Part I: Dynamics of a human riding a unicycle and its modeling by link mechanisms," *JSME Int. J. Ser. C, Dyn., Control, Robot., Des. Manuf.*, vol. 38, no. 2, pp. 249–259, 1995.

[17] H. Suzuki, S. Moromugi, and T. Okura, "Development of robotic unicycles," *J. Robot. Mechatronics*, vol. 26, no. 5, pp. 540–549, Oct. 2014.

[18] J. P. Meijaard, J. M. Papadopoulos, A. Ruina, and A. L. Schwab, "Linearized dynamics equations for the balance and steer of a bicycle: A benchmark and review," *Proc. Roy. Soc. A, Math., Phys. Eng. Sci.*, vol. 463, no. 2084, pp. 1955–1982, Aug. 2007.

[19] H. Dankowicz, *Multibody Mechanics and Visualization*. Cham, Switzerland: Springer, 2005.

[20] J. Xiong, N. Wang, and C. Liu, "Stability analysis for the whipple bicycle dynamics," *Multibody Syst. Dyn.*, vol. 48, no. 3, pp. 311–335, Mar. 2020.

[21] W. B. Qin, Y. Zhang, D. Takács, G. Stépán, and G. Orosz, "Nonholonomic dynamics and control of road vehicles: Moving toward automation," *Nonlinear Dyn.*, vol. 110, no. 3, pp. 1959–2004, Nov. 2022.

[22] E. J. Routh, *The Advanced Part of a Treatise on the Dynamics of a System of Rigid Bodies*. New York, NY, USA: Macmillan, 1884.

[23] A. Voss, "Ueber die differentialgleichungen der mechanik (about the differential equations of mechanics)," *Mathematische Annalen (Math. Ann.)*, vol. 25, pp. 258–286, Jan. 1885.

[24] A. M. Bloch, P. S. Krishnaprasad, J. E. Marsden, and R. M. Murray, "Nonholonomic mechanical systems with symmetry," *Arch. Rational Mech. Anal.*, vol. 136, no. 1, pp. 21–99, Dec. 1996.

[25] P. Appell, "Sur une forme générale des équations de la dynamique (on a general form of the equations of dynamics)," *J. für die reine und angewandte Mathematik (J. Pure Appl. Math.)*, vol. 121, pp. 310–319, Jan. 1900.

[26] J. W. Gibbs, "On the fundamental formulae of dynamics," *Amer. J. Math.*, vol. 2, no. 1, pp. 49–64, Mar. 1879.

[27] P. V. Voronets, "Ob uravneniyakh dvizheniya dlya negolonomnykh sistem (on the equations of motion of nonholonomic systems)," *Math. Collection*, vol. 22, no. 4, pp. 659–686, 1901.
[28] G. Hamel, "Nichtholonome Systeme höherer Art (Nonholonomic systems of a higher kind),"*Sitzungsberichte der Berliner Mathematischen Gesellschaft (Meeting Rep. Berlin Math. Soc.)*, vol. 37, pp. 41–52, Jan. 1938.
[29] T. R. Kane, "Dynamics of nonholonomic systems," *J. Appl. Mech.*, vol. 28, no. 4, pp. 574–578, Dec. 1961.
[30] F. Gantmacher, *Lectures in Analytical Mechanics*. Moscow, Russia: MIR Publishers, 1970.
[31] J. I. Neimark and N. A. Fufaev. *Dynamics of Nonholonomic Systems, of Translations of Mathematical Monographs*, vol. 33. Providence, RI, USA: American Mathematical Society, 1972.
[32] W. S. Koon and J. E. Marsden, "The Hamiltonian and Lagrangian approaches to the dynamics of nonholonomic systems," *Rep. Math. Phys.*, vol. 40, no. 1, pp. 21–62, Aug. 1997.
[33] S. Ostrovskaya and J. Angeles, "Nonholonomic systems revisited within the framework of analytical mechanics," *Appl. Mech. Rev.*, vol. 51, no. 7, pp. 415–433, Jul. 1998.
[34] A. M. Bloch, *Nonholonomic Mechanics and Control*. Cham, Switzerland: Springer, 2003.

Máté B. Vizi received the B.Sc. degree in mechatronic engineering, the M.Sc. degree in mechanical engineering modeling, and the Ph.D. degree from Budapest University of Technology and Economics, Budapest, Hungary, in 2016, 2018, and 2024, respectively.

He has a post-doctoral position at the University of Michigan, Ann Arbor, MI, USA. His research interests include nonlinear dynamics, control, and time delay systems.

Gábor Orosz (Senior Member, IEEE) received the M.Sc. degree in engineering physics from Budapest University of Technology and Economics, Budapest, Hungary, in 2002, and the Ph.D. degree in engineering mathematics from the University of Bristol, Bristol, U.K., in 2006.

He held post-doctoral positions at the University of Exeter, Exeter, U.K., and the University of California at Santa Barbara, Santa Barbara, CA, USA. In 2010, he joined the University of Michigan, Ann Arbor, MI, USA, where he is currently a Professor of mechanical engineering and civil and environmental engineering. From 2017 to 2018, he was a Visiting Professor of control and dynamical systems at California Institute of Technology, Pasadena, CA, USA. In 2022, he was a Distinguished Guest Researcher in applied mechanics at Budapest University of Technology and Economics, where he was a Fulbright Scholar from 2023 to 2024. His research interests include nonlinear dynamics and control, time delay systems, machine learning, and data-driven systems with applications to connected and automated vehicles, traffic flow, and biological networks.

Dénes Takács received the M.Sc. and Ph.D. degrees in mechanical engineering from Budapest University of Technology and Economics, Budapest, Hungary, in 2005 and 2011, respectively.

From 2011 to 2018, he was with the MTA-BME Research Group on Dynamics of Machines and Vehicles, Budapest, Hungary. Since 2018, he has been an Associate Professor at Budapest University of Technology and Economics. His research interests include tire and vehicle dynamics, nonlinear dynamics, and time delay systems.

Gábor Stépán received the M.Sc. and Ph.D. degrees in mechanical engineering from Budapest University of Technology and Economics, Budapest, Hungary, in 1978 and 1982, respectively, and the D.Sc. degree from the Hungarian Academy of Sciences, Budapest, in 1994.

He was a Visiting Researcher with the Mechanical Engineering Department, University of Newcastle upon Tyne, Newcastle upon Tyne, U.K., from 1988 to 1989, the Laboratory of Applied Mathematics and Physics, Technical University of Denmark, Kongens Lyngby, Denmark, in 1991, and the Faculty of Mechanical Engineering, Delft University of Technology, Delft, The Netherlands, from 1992 to 1993. He was a Fulbright Visiting Professor at the Mechanical Engineering Department, California Institute of Technology, Pasadena, CA, USA, from 1994 to 1995, and a Visiting Professor at the Department of Engineering Mathematics, Bristol University, Bristol, U.K., in 1996. He is currently a Professor of Applied Mechanics at Budapest University of Technology and Economics. His research interests include nonlinear vibrations in delayed dynamical systems and applications in mechanical engineering and biomechanics, such as wheel dynamics (rolling, braking, and shimmy), robotic force control, machine tool vibrations, human balancing, and traffic dynamics.

Dr. Stépán is a fellow of CIRP and SIAM. He is a member of the Hungarian Academy of Sciences and the Academy of Europe. He received the Delay Systems Lifetime Achievement Award of IFAC, the Caughey Dynamics Award, and the Lyapunov Award of ASME.